Icelandic
Meteorological Office

Veðurstofa
Íslands

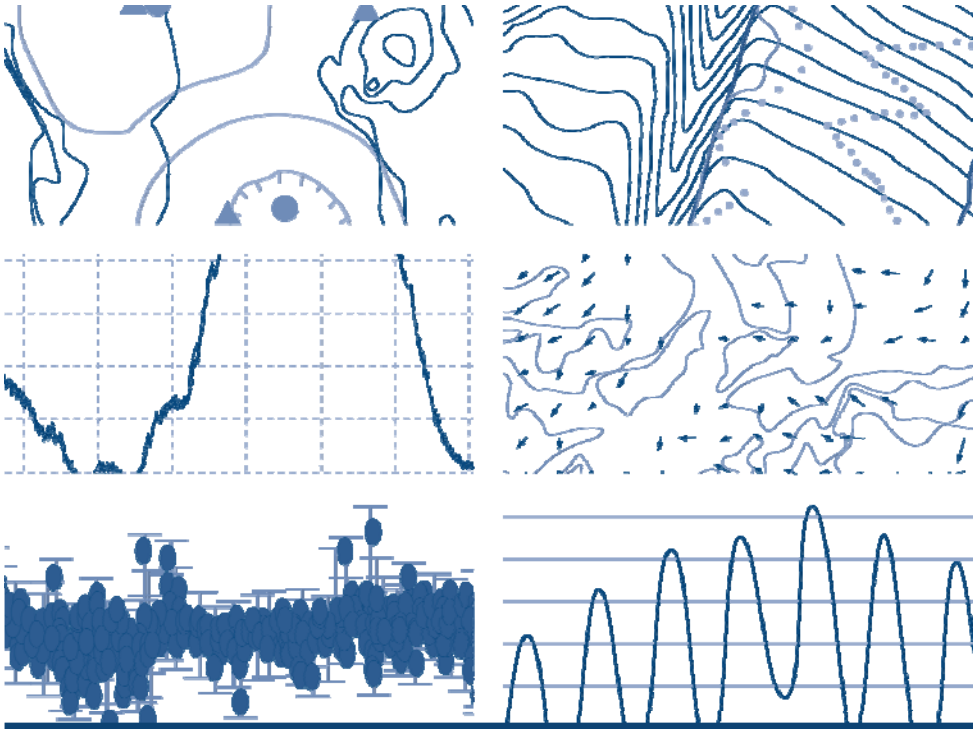

Attenuation relations for near- and far-field peak ground motion (PGV, PGA) and new magnitude estimates for large earthquakes in SW-Iceland

Gunnar Geir Pétursson
Kristín S. Vogfjörð

Skýrsla

VÍ 2009-012

Icelandic
Meteorological Office

Veðurstofa Íslands

Attenuation relations for near- and far-field peak ground motion (PGV, PGA) and new magnitude estimates for large earthquakes in SW-Iceland

Gunnar Geir Pétursson, Veðurstofu Íslands, nú Fjölbrautaskólanum við Ármúla
Kristín S. Vogfjörð, Veðurstofu Íslands

Skýrsla

Veðurstofa Íslands
Bústaðavegur 9
150 Reykjavík

+354 522 60 00
+354 522 60 06
vedur@vedur.is

VÍ 2009-012
ISSN 1670-8261

Veðurstofa Íslands

Keypage

Report no.:	Date.:	ISSN:	Public ☒ Restricted ☐
VÍ 2009-012	December 2009	1670-8261	**Provision:**

Report title / including subtitle	**Number of copies:**
Attenuation relations for near- and far-field peak ground motion (PGV, PGA) and new magnitude estimates for large earthquakes in SW-Iceland	25
	Pages: 43
Authors: Gunnar Geir Pétursson, Kristín S. Vogfjörð	**Managing director** Jórunn Harðardóttir
	Project manager: Kristín S. Vogfjörð
Project phase: Research, modelling of seismological data	**Project number:** 2811-0-0005

Report contracted for:
European Commission, under 6th Framework Project-'SAFER', Contract No. 036935.

Prepared in cooperation with:

Summary:
New attenuation relations for peak ground velocity (PGV) and peak ground acceleration (PGA) are developed for SW Iceland. The estimates of peak ground motion are retrieved from seismograms recorded on stations of the SIL seismic network, at 3 to 380 km distance from 46 earthquakes of local moment magnitude $3.3 \leq MLw \leq 6.5$. The relations are obtained by least-squares curve fitting of the squared sum of vertical- and horizontal-component measurements obtained from the stations. The relationships include both near-field and far-field effects, which enables realistic modeling of peak ground motion at epicentral distances between 0 and 380 km. Five events with teleseismically determined magnitudes are used to calibrate the attenuation, in order to correct the local magnitudes of the remaining events. The relations are compared with equations obtained for Iceland and other areas.

Keywords:
Seismic attenuation relations, Iceland, Peak ground velocity, Peak ground acceleration, Magnitude determination, Instrument response

Managing director's signature:

Project manager's signature:
Kristín S. Vogfjörð

Reviewed by:
SG

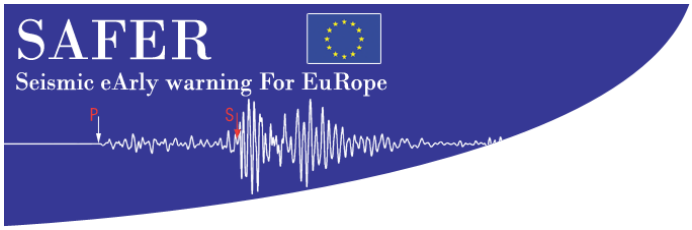

Project no. **036935**

Project acronym: **SAFER**

Project title: **Seismic eArly warning For EuRope**

Instrument : **Specific Targeted Research Project**

Thematic Priority: **Sustainable development, global change and ecosystem priority 6.3.iv.2.1: reduction of seismic risks**

D5.2 Improve PGA- and VGA-distance relations, determine long-term background seismic hazard estimate and derive clustering properties (space-time-magnitude) for SW Iceland.

SAFER Rannsóknaverkefnið

Í Evrópusamstarfsverkefninu SAFER (Seismic eArly warning For EuRope) var unnið að rannsóknum og þróun á rauntímaúrvinnslu jarðskjálftabylgna um leið og þær berast í mælistöðvar í því markmiði að þróa ferla sem geta nýst til viðvarana og viðbragða áður en stærstu og skæðustu jarðskjálftabylgjurnar berast til viðkvæmra mannvirkja eða þéttbýliskjarna, þar sem þær geta skapað hættu. Þátttakendur voru frá helstu jarðskjálftarannsóknastofnunum Evrópu og þeim löndum álfunnar þar sem jarðskjálftavá er mest. Veðurstofa Íslands var þátttakandi í verkefninu og vann að þróun rauntímaferla fyrir bráðaskjálftaviðvörun (e. seismic early warning) á Suðvesturlandi. Helstu niðurstöður rannsóknanna voru settar fram í nokkrum smáskýrslum (e. deliverables), sem var skilað sem afurðum Veðurstofunnar í verkefninu. Þessum smáskýrslum er safnað saman í tvær skýrslur, þar sem sú fyrri inniheldur niðurstöður um dvínun hraða og hröðunar með fjarlægð frá upptökum jarðskjálfta, en sú síðari er um: 1) þróun sjálfvirkrar kortlagningar sprungna í nærrauntíma, 2) rauntímamat á stærð jarðskjálfta byggt á ráðandi tíðni í P-bylgjum (ElarmS), 3) samband milli skjálftaáhrifa og mesta hraða og hröðunar, 4) þróun sjálfvirkra, rauntíma „alert“ korta og hristingskorta (ShakeMap) fyrir jarðskjálfta, 5) undirbúning rauntímakortlagningar á eftirskjálftavá, og 6) rauntímakortlagningu spennuútlausna skjálfta. Upplýsingar um SAFER verkefnið má finna á vefsíðunni: http:// www.saferproject.net/.

Contents

List of figures

List of tables

1 Abstract

Forty six earthquakes in SW Iceland of local moment magnitude, M_{Lw}, between 3.3 and 6.5 are selected from the data base of the national seismic network, SIL and used to develop new attenuation relations for peak ground velocity (PGV) and peak ground acceleration (PGA). The relations are developed for the squared sum of vertical- and horizontal-component measurements retrieved from stations at 3 to 380 km distances.

Magnitudes of events of M > 3 are generally underestimated by the SIL system software, but by relying on teleseismic moment magnitude estimates (Global CMT M_w) of five of the six largest digitally recorded earthquakes in SW Iceland to calibrate the attenuation, the local moment magnitude estimates (M_{Lw}) of the events under study can be corrected. The improved magnitude estimates are used to develop attenuation relationships for PGV and PGA. These relationships take into account near-source effects, which enables realistic modeling of peak ground motion at epicentral distances between 0 and 380 km.

2 Introduction

The Mid-Atlantic Rift crosses Iceland from southwest to northeast, with rifting and transform motion taking place at the plate boundary, leading to volcanic activity and earthquakes. The geological units are shown on the map in Figure 1. The Western Volcanic Zone (WVZ) encompasses the part of the rift which enters land at the western tip of Reykjanes Peninsula (RP), runs east along the peninsula to the Hengill region, where it turns northward. East off the Hengill region the rifting shifts approximately 90 km eastward along the South Iceland Seismic Zone (SISZ), to the Eastern Volcanic Zone (EVZ). Most large earthquakes in southern Iceland occur on N-S oriented right-lateral, strike-slip faults contained within the 15-km-wide, left-lateral SISZ shear zone. These earthquakes can be as large as M7. Significant earthquakes can also occur on N-S strike-slip faults on the RP. The SISZ region is rather densely populated farmland containing a few small towns, exposing a few thousand people to the hazards of strong to severe Earth shaking. The WVZ is mostly uninhabited, but the proximity of the capital, Reykjavík, to the WVZ and the SISZ, however subjects tens of thousands of people to moderate effects of shaking. Major power-lines to the capital, telecommunications and roads are also susceptible to damage.

The goals in SAFER include installation of real-time aftershock hazard mapping (Gerstenberger et al., 2005) and ShakeMap (Wald et al., 1999) for SW Iceland. These can enable fast estimation of seismic hazard and potential damage after an earthquake, which can be of great value for disaster management. Necessary support for the generation of such maps is the development of attenuation relations for peak ground velocity and peak ground acceleration in the region. In order to develop attenuation relationships valid for PGV and PGA in SW Iceland, 46 earthquakes from the region were chosen from the SIL seismic catalog of the Icelandic national seismic network (Jakobsdóttir et al., 2002). The events are in the magnitude range $3.3 \leq M_{Lw} \leq 6.5$, where M_{Lw} is a local moment magnitude (see Appendix A) obtained from spectral analysis of P- and S-waveforms (Rögnvaldsson and Slunga, 1993). Event locations are shown in Figure 1 and listed in Table 2. All the events are shallow and most occurred in the Hengill region in 1997 and 1998, at the intersection of the SISZ and the WVZ. Seven events are located

on the Reykjanes Peninsula and six in the SISZ. Events in the SISZ are mostly from the year-2000 seismic sequence, which also contains the three largest events in the data set (Jakobsdóttir et al., 2002; Hjaltadóttir and Vogfjörd, 2005).

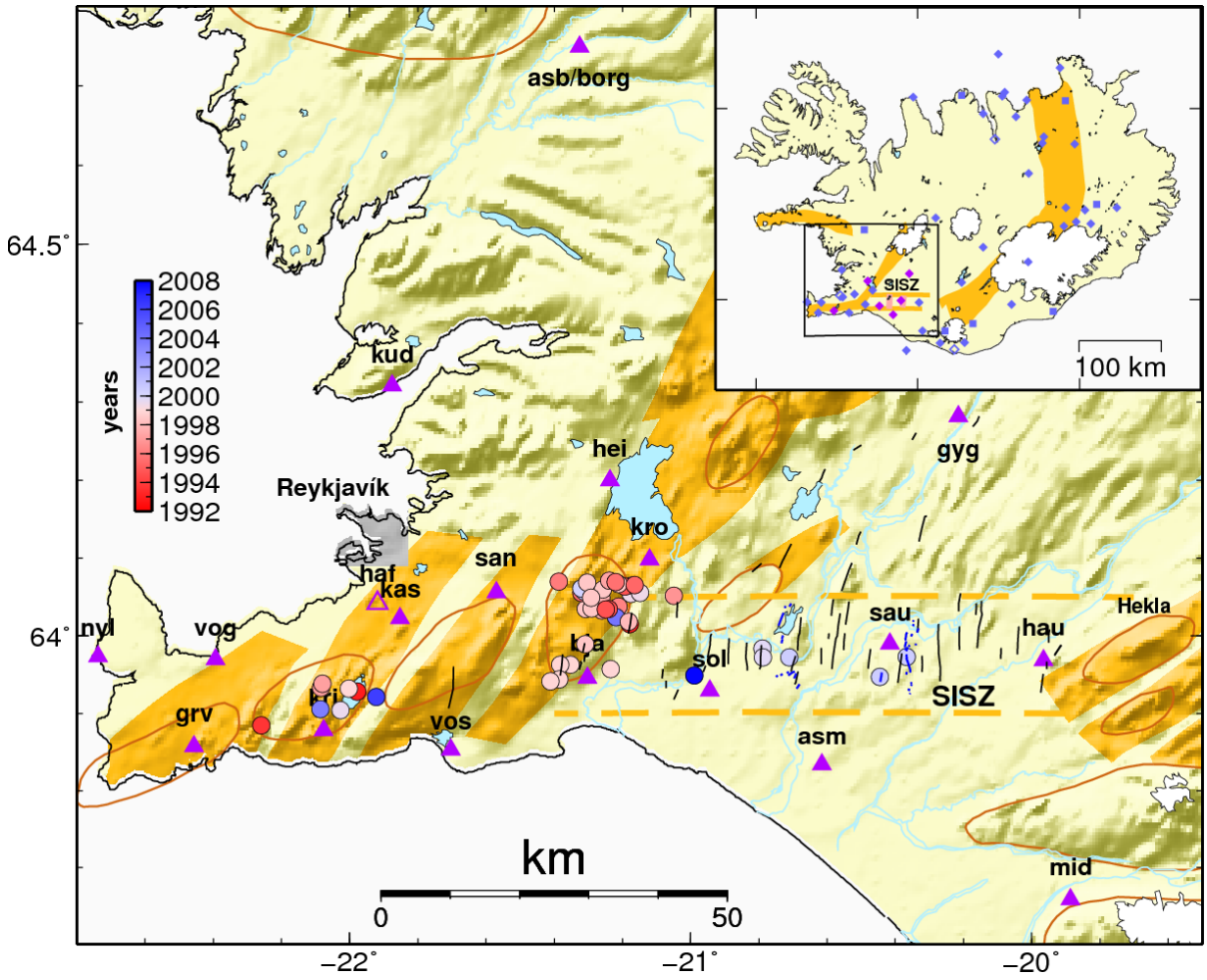

Figure 1. Map of SW Iceland showing the epicenters of the 46 earthquakes used in the study, color coded according to origin time. The time scale is shown on the left. Most of the events cluster in the Hengill region, in the center of the map, but several are also located on Reykjanes Peninsula, south of Reykjavík and to the east, in the SISZ. Volcanic zones (solid orange), outline of the SISZ (dashed orange), and seismic stations in the SIL network (purple triangles) are indicated, as well as traces of some previously mapped surface faults (black lines). The inset in the upper right corner shows locations of seismic stations in the SIL network.

An earlier estimate of PGA attenuation with distance was made by Halldórsson and Sveinsson (2003), for the development of the Eurocode 8 standard. It was based on 131 observations of horizontal acceleration from 22 earthquakes (18 in SW Iceland and 4 in N Iceland). The events were of magnitudes between 4.5 and 6.5, and recorded between 1986 and 2000 on the Earthquake Engineering Research Center's network.

A previous analysis by Ágústsson *et al.* (2008) of PGV and PGA far-field attenuation included the present data set, in addition to earthquakes on the Reykjanes Ridge (RR) and Mýrdalsjökull volcano in south central Iceland. On closer inspection, the estimation of PGV and PGA turned out to be significantly flawed. Therefore, the data was reanalyzed, and the events on the RR and in Mýrdalsjökull left out because of uncertainties in magnitude estimates for these events.

3 Data and data processing

The national seismic network, SIL is composed of 3-component velocity meters, mostly short-period Lennartz sensors; 7 with a corner frequency at 1 Hz and over 35 with a corner at 0.2 Hz. Through the years there have also been 6 to 8 broad-band sensors distributed around the country. These include CMG-3T, CMG-40T, CMG-ESP and STS2, with corner frequencies at 0.008 and 0.033 Hz. A large portion of the sites are equipped with short-period Nanometrics RD3 digitizers with a corner frequency around 0.5 Hz and the remaining have CMG-DM24 digitizers, with a flat response. The maximum amplitude of the stations varies between 0.3 cm/s and 1.25 cm/s. Therefore stations located in the near-field of earthquakes are often saturated and unusable. The default sampling rate of the system is 100 Hz, but a few waveforms are sampled at 20 Hz.

The 46 earthquakes were selected on the basis of magnitude and number and quality of usable waveforms. The waveforms were then analyzed using the SAC software package (Seismic Analysis Code; Goldstein and Snoke, 2005). First, instrument responses were removed from the traces. Upon instrument removal the waveforms were high-pass filtered: From the short-period traces frequencies below 0.15 Hz were filtered out, while in the traces from the broad-band sensors (for all types of digitizers), frequencies below 0.1 Hz were filtered away. Then, the maximum of the squared sum of all three components was saved as PGV for the velocity records. Acceleration records were obtained by differentiating the velocity traces after instrument removal and then saving the maximum of the 3-component squared sum as PGA. Data with 20 Hz sampling were not used for the maximum acceleration estimates, and data from the Lennartz 1 Hz sensors were not used at distances greater than 100 km. The resulting parameter data set consisted of 865 PGV estimates and 823 PGA estimates, at magnitudes within the range $3.3 \leq M_{Lw} \leq 6.5$ and epicentral distances from 3 to 380 km.

Focal mechanisms and seismic moment (M_0) are calculated for all recorded earthquakes in Iceland. They are obtained by grid searching through all combinations of strike, dip and rake, matching observed first-motion polarities as well as amplitudes of P- and S-waves estimated from spectral analysis (Rögnvaldsson and Slunga, 1993). A local moment magnitude, M_{Lw}, is derived from the estimated seismic moment. However, unlike the moment magnitude scale of Hanks and Kanamori (1979), this local magnitude scale is not a linear function of $\log_{10}(M_0)$ (see Appendix A or Slunga *et al*. 1984). Furthermore, the SIL system software is designed to analyze microseismicity and is prone to underestimate the seismic moment of events greater than M~4. Therefore, magnitudes of all events were recalculated, after calibration with the teleseismically determined, Global CMT moment magnitude, M_w of five reference events. The attenuation models were then fitted to the derived M_w of all 46 events.

The PGV and PGA estimates as a function of epicentral distance and recalculated magnitude, here denoted by $M_w(v)$ were analyzed using the R statistical package (R Development Core

Team, 2007). The model candidates were fitted using least-squares methods such as lm (linear model) and nlm (non-linear minimization), which are available in R. Non-linear minimization (Dennis and Schnabel, 1983; Schnabel *et al*, 1985) was used in cases where non-linear models were fitted to the data set. This method computes numerical derivatives in its search for minimum of the sum of squared log-residuals:

$$\sum_i \{\log_{10}(PGX_i) - f(M_i, r_i, ...)\}^2,$$

where PGX stands for either PGV or PGA and the term f(M,r,...) denotes the model in question as a function of magnitude and epicentral distance that approximates $\log_{10}$(PGX).

4 Recalculation of magnitudes and pgx-distance relations without near-source effect

Before the attenuation relationships can be derived, the magnitude errors in the original data set must be corrected. That these errors are significant, is demonstrated in Table 1. There, M_w values calculated from the seismic moment estimates of the SIL system software, are compared to those calculated from the seismic moment obtained from the Global Centroid Moment Tensor solutions (CMT) (Dziewonski *et al.* 1983). The M_w values derived from the SIL system for the 4th, 5th and 6th largest earthquakes in the data set are 4.4 for all three events, while the corresponding Global CMT estimates are 5.1, 5.1 and 5.4, or greater by 0.7 to 1.0 magnitude units. A procedure was therefore set up to re-determine the magnitudes for the data set, using the five available Global CMT magnitude estimates for calibration. This means extrapolating the relationship from the smallest CMT magnitude available, M_w=5.1 down to magnitude M_w=3.

The peak ground velocity and acceleration data are fitted to a multiple general linear regression model of the form:

$$\log_{10}(PGX) = a \cdot \log_{10}(r) + \sum_{i=1}^{N} C_i E_i \ ,$$

where r is the epicentral distance in km, N is the number of earthquakes in the data set and E_i is 1 for event number i and 0 otherwise. Different C_i's are thus found for different events, while a is determined for the whole set. This method of using dummy variables E_i is a well known technique in regression analysis (see Weisberg, 1980) and was for example used by Joyner and Boore (1981) in the derivation of attenuation formulas for California.

Table 1. Origin time, location and magnitude estimates of the five calibration events. M_{Lw} is the local moment magnitude from the SIL catalog. M_0^{SIL} is the seismic moment determined by the SIL system software. M_w is the general moment magnitude and M_0^{CMT} is the seismic moment of the teleseismically determined Global CMT solution.

Date (yyyymmdd)	Origin time (hhmmss.ms)	Latitude (˚N)	Longitude (˚W)	MLw (M0 SIL)	Mw (M0SIL)	MLw (M0CMT)	Mw (M0CMT)
20000621	005146.985	63.973	20.711	6.6*)	6.6	6.5	6.4
20000617	154040.998	63.973	20.367	6.4*)	6.2	6.5	6.5
19981113	103834.415	63.963	21.352	5.1	4.4	5.6	5.1
20030823	020011.787	63.905	22.085	5.0	4.4	5.7	5.1
19980604	213653.811	64.036	21.290	5.0	4.4	5.9	5.4

*) These values, obtained by manually determining the amplitudes of the waveform spectra, are the largest estimates found. The magnitudes obtained by the routine solutions are less than 6.0.

In the second step of this procedure, the C_i values found in the first step are fitted to a set of parameters describing the function h:

$$C_i = h(M),$$

where h is usually a first or second order polynomial. One advantage of this method is the possibility of estimating M when h is known.

The five C_i values determined in step one by fitting the PGV values of the five reference earthquakes, are used to determine a magnitude scale, assuming that h is a linear function of M_w and that the magnitude coefficient is equal to one, analogous to the Richter scale. The C_i values are thus fitted to the function:

$$C_i = b \cdot M_{w_i}^{CMT} + c \ , \ i = 1,\ldots 5,$$

with $b = 1$ and the parameter c estimated by least squares to be -4.88. Having determined c, the magnitudes of all earthquakes in the data set are recalculated according to:

$$M_w(v)_i := C_i + 4.88$$

With a determined to be -1.63 in the first step, the resulting log-linear attenuation relationship becomes:

$$\log_{10}(PGV) = -1.63 \cdot \log_{10}(r) + M - 4.88, \qquad \text{(A)}$$

Equation A is similar to the present velocity-attenuation formula used at IMO to estimate local magnitude M_L, which is given by:

$$\log_{10}(\max velocity) = -2.1 \cdot \log_{10}(r) + M - 4.8$$

where max *velocity* is determined in a 10 second time window around the S-wave arrival after a 1.5 Hz high-pass (Gudmundsson et al., 2006). This equation has the same magnitude coefficient and a similar *c* coefficient as equation A, but differs in the distance parameter, which may be due to the effect of the 1.5 Hz high-pass.

The CMT M_w estimates are plotted against ($C_i - c$) in Figure 2 (red squares), together with the scale fitted to the five data points (green line). The $M_w(M_0^{SIL})$ of the whole data set are also shown on the figure. Setting the magnitude parameter, *b* equal to 1 fits well with the CMT magnitude estimates and with the magnitudes of the smallest events in the data set, but not so well with those of the larger events, presumably due to their underestimated seismic moments. The line also fits adequately with magnitude estimates of several small events belonging to an earthquake swarm on the Reykjanes Peninsula in January 2008, which were recorded on a nearby station. Extrapolating the scale to magnitude values much smaller than M_w5 therefore is probably not a source of significant errors.

Table 2 lists the origin times and locations of the 46 earthquakes in the data set, together with the original magnitude estimates ($M_{Lw}(M_0^{SIL})$, $M_w(M_0^{SIL})$), and the magnitudes determined from equation A ($M_w(v)$, $M_{Lw}(v)$). The events from Table 1 are written in bold in Table 2.

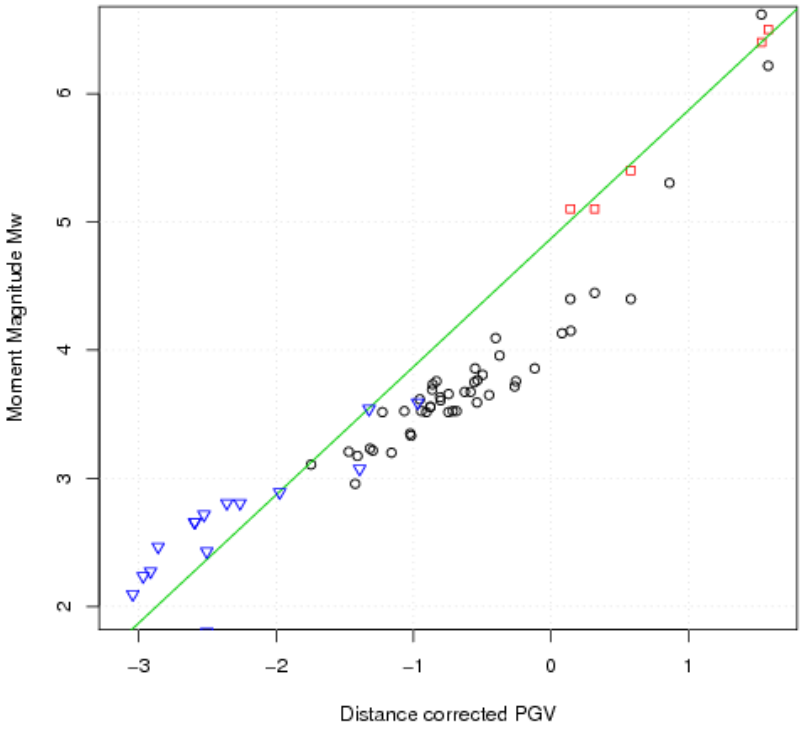

Figure 2. FiCMT-moment magnitude estimates (red squares) plotted against distance corrected PGV, or ($C_i - c$). The magnitude scale fitted through the five events is shown by the green line. $M_w(M_0^{SIL})$ of the remaining data set are shown with black circles. The line fits adequately to the smallest magnitude values of the data set, as well as to additional data from small events on Reykjanes Peninsula, shown with blue triangles. The deviation of the larger events in the data set from the green line is presumably due to underestimation of seismic moment by the SIL system.

Table 2. Origin times and locations of the events in the data set. Four magnitude columns are shown: Original local moment magnitude $M_{Lw}(M_0^{SIL})$; revised M_{Lw} value obtained in this study; M_w corresponding to the initial M_0^{SIL} estimate; the revised M_w value. Last two columns show the respective distance coefficients, describing the decay of PGV and PGA. Events written in bold letters are from Table 1.

yyyymmdd	hhmmss.ms	Lat.(°N)	Lon.(°W)	Depth	$M_{Lw}(M_0^{SIL})$	M_{Lw}(v)	$M_w(M_0^{SIL})$	M_w(v)	a(v)	a(a)
20071120	184854.3	63.949	20.989	1.84	3.3	3.9	3.0	3.5	-1.7	-2.0
19990720	060402.1	63.904	22.027	5.37	3.5	3.5	3.1	3.1	-1.7	-2.2
19990525	180305.2	64.054	21.175	5.55	3.6	4	3.2	3.5	-1.6	-2.0
19951227	042606.8	64.070	21.387	0.04	3.6	4.2	3.2	3.7	-1.1	-1.5
20000418	194907.7	64.061	21.321	3.87	3.6	3.9	3.2	3.4	-2.0	-2.5
19980603	184609.0	64.067	21.211	3.48	3.7	4.1	3.2	3.6	-1.6	-1.9
19930919	100030.8	63.885	22.260	5.34	3.7	4.1	3.2	3.6	-1.7	-2.2
19980604	220440.2	64.050	21.291	4.83	3.8	4.4	3.3	3.9	-1.6	-2.0
19950820	165704.0	64.069	21.221	2.13	3.8	4.4	3.3	3.9	-1.7	-1.3
19950723	092855.1	64.056	21.321	5.15	4.0	4.2	3.5	3.6	-1.9	-2.5
19970223	084503.3	63.939	22.079	4.29	4.0	4.7	3.5	4.1	-1.7	-2.1
19970824	032001.7	64.050	21.262	4.56	4.0	4.5	3.5	4	-1.8	-2.2
19950430	005759.3	64.066	21.164	3.35	4.0	4.8	3.5	4.2	-1.2	-1.6
19971229	103731.3	64.019	21.182	5.21	4.0	4.4	3.5	3.8	-1.5	-1.9
19980604	122327.4	64.035	21.308	4.16	4.0	4.5	3.5	3.9	-1.7	-2.0
19981114	043639.7	63.942	21.410	5.30	4.0	4.8	3.5	4.2	-1.0	-1.5
19940817	062930.0	64.064	21.193	2.95	4.1	4.6	3.6	4	-1.6	-1.7
19970223	003548.2	63.934	22.084	4.58	4.1	4.6	3.6	4	-1.6	-2.1
19940819	191841.6	64.034	21.249	1.46	4.1	5	3.6	4.3	-1.6	-1.6
19990928	215020.0	63.984	20.790	4.89	4.1	4.7	3.6	4.1	-1.9	-2.4
19980603	232348.8	64.065	-21.173	4.34	4.1	4.5	3.6	3.9	-1.5	-1.8
19981130	104116.2	63.932	-22.002	5.62	4.2	4.7	3.6	4.1	-1.7	-2.2
19940820	164025.9	64.035	-21.241	1.66	4.2	5	3.6	4.4	-1.4	-1.8
20000617	162404.4	64.058	-21.312	4.09	4.2	4.7	3.7	4.1	-1.8	-2.3
19921120	102833.4	63.929	-21.978	6.79	4.2	4.9	3.7	4.3	-1.5	-1.9
19981114	042113.8	63.944	-21.386	4.19	4.2	4.8	3.7	4.2	-1.4	-2.0
20040107	232525.3	64.024	-21.219	6.21	4.2	4.6	3.7	4	-1.5	-1.9

Continues, next page

yyyymmdd	hhmmss.ms	Lat.(°N)	Lon.(°W)	Depth	$M_{Lw}(M_0^{SIL})$	$M_{Lw}(v)$	$M_w(M_0^{SIL})$	$M_w(v)$	a(v)	a(a)
19921227	122322.2	64.016	-21.179	0.76	4.3	5.2	3.7	4.6	-1.5	-2.0
19960314	053456.7	64.038	-21.212	4.09	4.3	4.6	3.7	4	-1.9	-2.1
19990525	131940.0	64.056	-21.149	5.27	4.3	4.9	3.7	4.3	-1.7	-2.0
19980603	064741.9	64.060	-21.258	4.13	4.3	4.6	3.8	4	-1.8	-2.0
19980604	190444.8	64.069	-21.303	3.99	4.3	5.2	3.8	4.6	-1.4	-1.9
19970412	230444.3	64.072	-21.238	3.73	4.3	5	3.8	4.3	-1.7	-1.9
19961014	205957.8	64.052	-21.049	4.23	4.4	5	3.8	4.4	-1.7	-2.0
19980604	225957.1	63.990	-21.308	3.09	4.4	5.4	3.9	4.8	-1.5	-
19981113	104631.2	63.963	-21.382	9.49	4.4	4.9	3.9	4.3	-1.7	-2.0
19990927	160115.0	63.973	-20.788	5.97	4.5	5.1	4.0	4.5	-1.7	-2.2
20060306	143154.5	63.921	-21.922	8.07	4.7	5.1	4.1	4.5	-1.8	-2.2
19970824	030422.1	64.033	-21.261	5.37	4.7	5.5	4.1	5	-1.6	-2.2
19981114	142406.9	63.957	-21.235	4.40	4.8	**5.6**	4.2	5	-1.4	-1.7
19980604	**213653.8**	**64.036**	**-21.290**	**5.90**	**5.0**	**5.9**	**4.4**	**5.5**	**-1.3**	**-2.1**
20030823	**020011.8**	**63.905**	**-22.085**	**3.73**	**5.0**	**5.6**	**4.4**	**5**	**-1.7**	**-1.9**
19981113	**103834.4**	**63.963**	**-21.352**	**5.00**	**5.1**	**5.7**	**4.4**	**5.2**	**-1.5**	**-2.0**
20000617	154250.6	63.943	-20.460	6.03	5.8	6.1	5.3	5.7	-1.1	-1.9
20000617	**154041.0**	**63.973**	**-20.367**	**6.35**	**6.4**	**6.5**	**6.2**	**6.4**	**-1.3**	**-2.1**
20000621	**005147.0**	**63.972**	**-20.711**	**5.00**	**6.6**	**6.5**	**6.6**	**6.5**	**-1.3**	**-2.2**

A second advantage of the two step regression applied is that when the M_i are known, errors in the magnitude estimate do not affect the estimation of the distance parameter *a*. When both the distance (*a*) and the magnitude (*b*) parameters are fitted in a one step regression, a positive correlation between log distance and magnitude can result in large errors in the fitted parameters *a* and *b*. In their paper, Fukushima and Tanaka (1990) argue that a high correlation between log distance and magnitudes are responsible for consistently low distance parameters in older Japanese attenuation studies. Using a one step regression model, their distance parameter, *a,* was estimated as 1.19, compared to 1.78 in the 'two step stratified' version. In our data set the correlation coefficient between the two is relatively low, when using the underestimated magnitudes M_i and the changes between the one step and the two step regression methods is less than 1% for the coefficients *a* and b. In Figure 3 the magnitudes are plotted against log-distance.

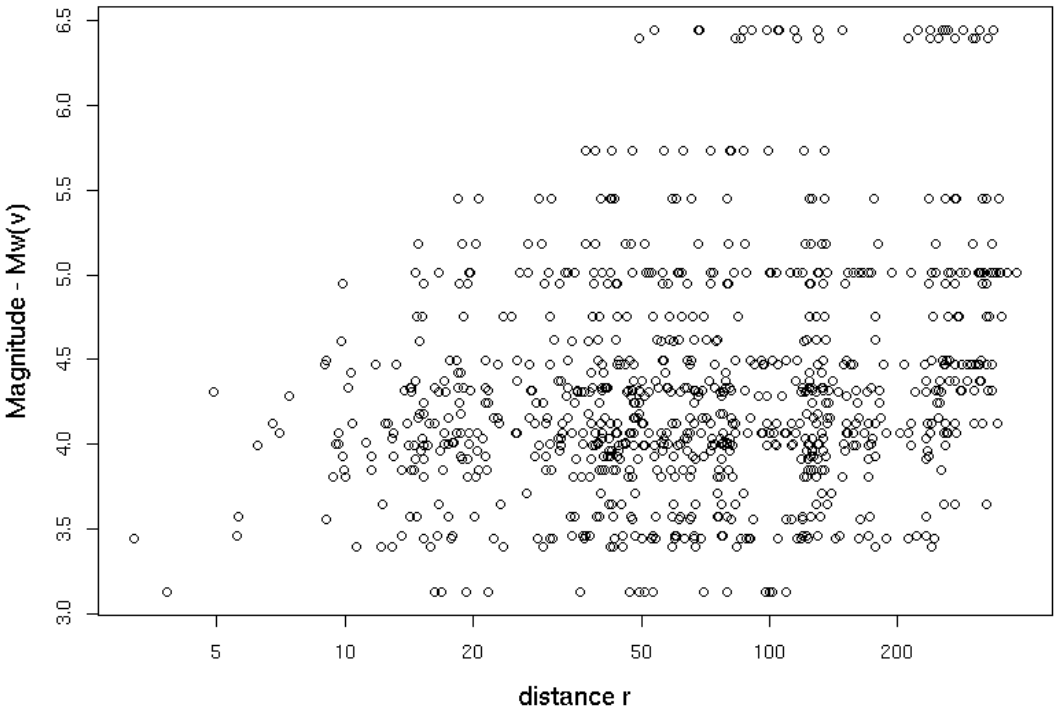

Figure 3. Corrected magnitudes, $M_w(v)$ plotted against log distance. The coefficient of correlation between $M_w(v)$ and log distance is 0.24. High correlation coefficients have been shown to affect parameter estimates in one step regression methods (see Fukushima and Tanaka, 1990).

The C_i values were also calculated from the derived PGA values. Instead of constructing another magnitude scale based on acceleration it was decided to use the available new estimates $M_w(v)$ to build a PGA relationship that would give very similar results as model A. Due to the more complicated relationship between C_i and $M_w(v)$ in the acceleration case, a second order polynomial was chosen as the functional form of h and thus through the least-squares method we estimated the parameters b, c and d according to:

$$C_i = d \cdot M_w^2(v) + b \cdot M_w(v) + c$$

and obtained the following least squares solution:

$$\log_{10}(PGA) = -2.08 \cdot \log_{10}(r) - 0.0431 \cdot M^2 + 1.21 \cdot M - 2.96\,, \qquad \text{(B)}$$

where M is the approximated moment magnitude and a=-2.08 had already been estimated from the first step. This second order fit through the estimates, $M_w(v)$ is shown in Figure 4**,** along with the original estimates $M_w(M_0^{SIL})$. The coefficient of the magnitude term in equation A was chosen to be 1, in other words the derivative of the right hand side with respect to M is 1, a constant. In equation B this derivative is -0.0862 M+1.21, so it changes in our magnitude range (3 - 6.5) from 0.95 to 0.65. In the studies of Joyner and Boore (1981), Halldórsson and Sveinsson (2003), and Bindi *et al.* (2006), these derivatives produce smaller values, 0.25, 0.48 and 0.53, respectively. These differences can be explained by the saturation of the relation between PGA and magnitude for large earthquakes like the ones considered in these three

studies; they used events in the 5–7.7, 4.1–6.6 and 4–6 magnitude range, respectively. This saturation seems to be recognized in our dataset since *d* has a negative value in model B.

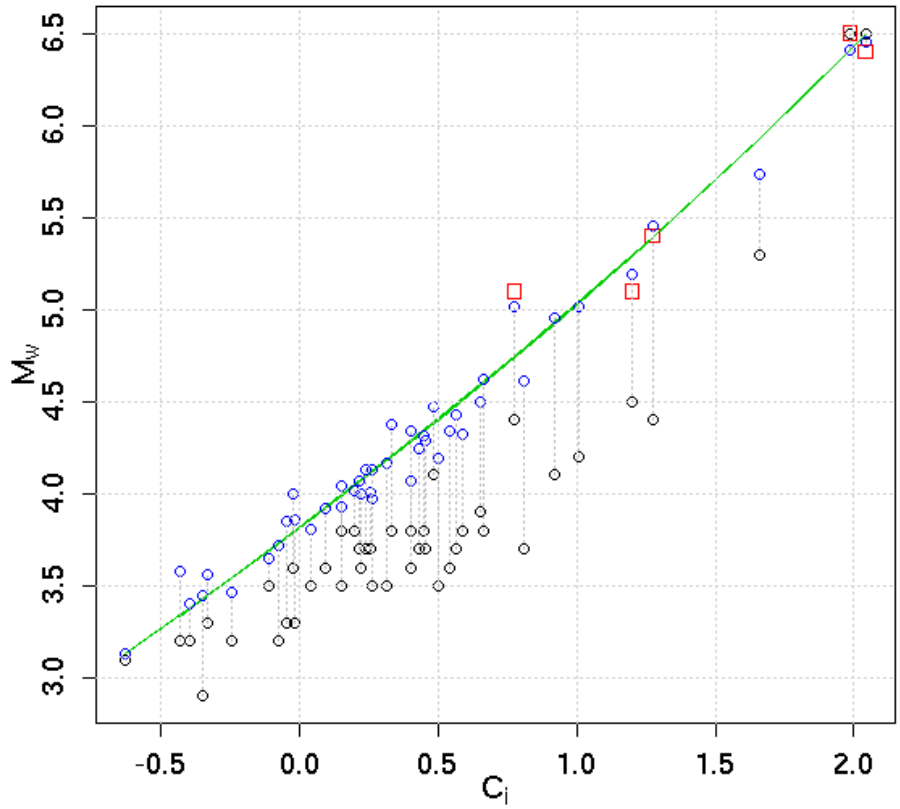

Figure 4. Magnitude estimates as a function of C_i. Red boxes are CMT estimates, blue and black dots are $M_w(v)$ and $M_w(M_0^{SIL})$ estimates, respectively. The green curve shows the fit of the second order polynomial through the $M_w(v)$ estimates.

The standard deviation of errors, defined as

$$\sqrt{\frac{1}{N}\sum_i \left\{\log_{10}(PGX_i) - a\log_{10}(r) - d\cdot M^2 - b\cdot M - c\right\}^2},$$

was 0.224 for the velocity and 0.304 for acceleration (*d* is 0 and *b* is 1 in the case of PGV). The difference in the standard deviation can be explained by the fact that the PGV model was fitted using 48 parameters, 46 of which were the new magnitude estimates, while the PGA model had only 4 parameters. No weighting scheme was used for the fitting of this regression model so that all measurements had equal weights.

Due to the decrease in dominant frequency with event magnitude and the increase in seismic wave attenuation with frequency we examined the dependence in the data set of the distance coefficients, *a* on magnitude. The distance parameter found when each earthquake is fitted to a model of the form

$$\log_{10}(PGX) = a\cdot\log_{10}(r) + D.$$

is shown in the last two columns of Table 2. Clearly $a(v)$, the velocity distance-coefficient, increases with magnitude while $a(a)$, the acceleration distance-coefficient, seems to have a somewhat more scattered and complicated relationship with magnitude. The magnitude estimates $M_w(v)$ were not found from the above formula where a differs from earthquake to earthquake. When the above model is fitted for each earthquake the values a and D are unstable as indicated by the outliers in the last two columns of table 2. Indeed, for some of the earthquakes, there are as few as 7 observations available to estimate the two parameters (like event number 4 in Table 2).

5 Other predictor variables

Comprehensive measurements of site responses at the seismic stations are not available and therefore similar predictor variables to those used by Joyner and Boore (1993) and Boore *et al.* (1997) cannot be included in the model.

In southwest Iceland, large earthquakes usually occur on north-south faults and many of the larger events in the data set share this mechanism. The effect of radiation pattern on the model parameters was therefore examined. A radiation pattern variable was constructed, such that all earthquakes were assumed to take place on north-south striking, vertical strike-slip faults. Interestingly, the fitted parameter multiplied with the radiation pattern term was close to 1, as theory predicts and the residual error was significantly reduced. However, inclusion of the variable resulted in a worse fit for some of the earthquakes as one would expect. Since all the earthquakes do not share the same, or similar fault orientation and mechanism, the variable was omitted from the chosen model.

6 Amplitude variations between stations and instrument type

With such a varied combination of instruments as the SIL network contains it is important to examine whether the different types of instruments are affecting the results. In fact, some of the stations in the network gave significantly different results compared to the rest. In Figures 5 and 6 the ratios of observed PGX and the two-step stratified predicted PGX is plotted for all observations at each recording station. Ratios colored red in Figure 5 are from short-period stations (Lennartz 1 Hz sensors and Nanometrics RD3 0.5 Hz digitizers) at epicentral distances greater than 100 km. These were omitted from the data set due to the lack of lower frequencies, caused by the instrument responses and the nature of the attenuation effects.

Some variations in the PGV and PGA values between recording stations are apparent in Figures 5 and 6, where some stations show significantly lower values than predicted; one such station being **hla** in northern Iceland. This is due to the short-period instrument type, Lennartz 1 Hz + RD3 and the approximately 250 km epicentral distance. The instrument combination filters away lower frequencies, which after the long propagation path cannot be completely regained by the instrument removal. Other stations with Lennartz 1 Hz + RD3 instruments are **asm**, **gyg**, **hei**, **kri**, **sau skh** and **sol**. They are all within 130 km epicentral distance so the low frequencies are not entirely lost in the instrument. Data from station **hla** are omitted from the data set.

Another station with diminished seismic amplitudes is **hve** in central Iceland, where the consistently small values are most likely due to strong attenuation effects on wave propagation paths along the Western Volcanic Zone. The same applies to stations **ada**, **bru** and **mok**, located around 300 km distance north of the Vatnajökull ice cap (Figure 1). Propagation paths to the stations go through the crust and upper mantle of the Eastern Volcanic Zone, at the location of the center of the mantle plume under Iceland. Crustal structure also affects amplitudes at station **snb** in south Iceland, mostly at 130 km epicentral distance. The station consistently exhibits higher values than predicted, due to strong Moho reflections in wave trains from the Hengill region (Figure 1).

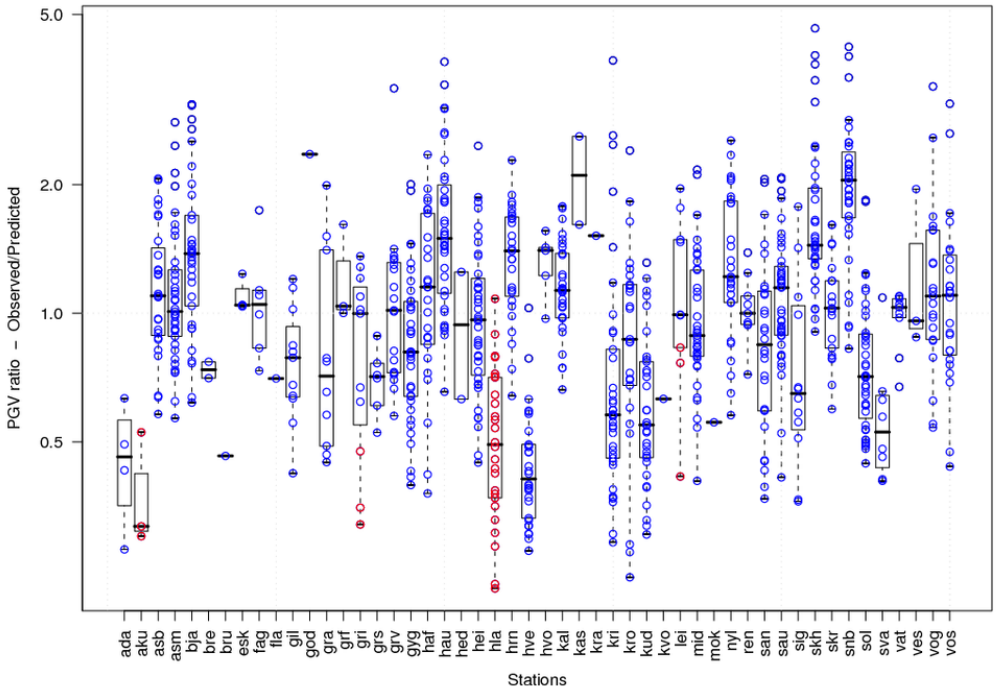

Figure 5. Observed/predicted PGV residuals for each station. Red circles represent data omitted from the data set, since they were measured far away from the epicenter with a short-period, 1 Hz+RD3 type instrument. Thick lines indicate the median.

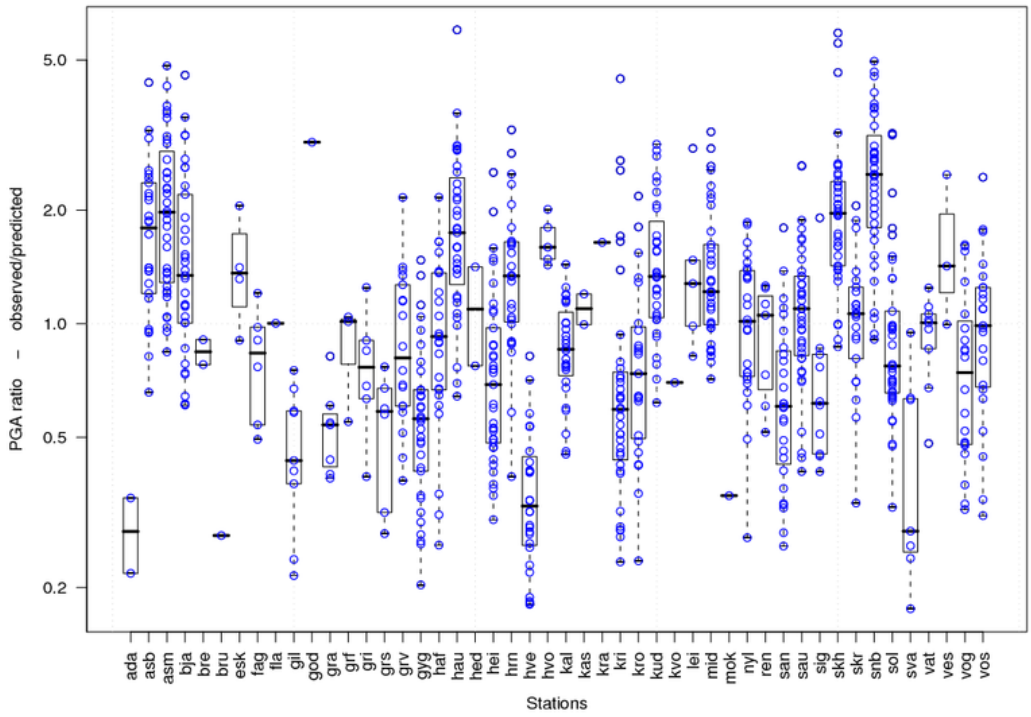

Figure 6. Observed/predicted PGA residuals for each station.

There is some variation in the distribution of observed/predicted PGV ratios as a function of instrument combination, as is shown in Figure 7. The medians of ratios from the broad-band digitizers (G24) are close to one, but the lowest median values are obtained at stations with short-period digitizers (RD3) in combination with either 1-Hz short-period (LE1) sensors, or broad-band (BB) sensors. The reason for the low ratios in the LE1-RD3 combination is obviously failure to retrieve all the low frequency amplitude through instrument response removal. The cause of the lower ratios at the broad-band stations however is the epicentral distance and resulting attenuation. This can be seen in Figure 8, where the ratios are plotted as a function of distance. The figure shows that most of the affected stations are at distances greater than 200 km (black circles). The extremely low values at 130 km distance are from station ***hve***. Figure 8 also shows that the residuals are not equally distributed with distance. Apart from the large ratios at 110 km distance, caused by Moho reflections, the ratios are generally lower at distances grater than ~100 km. Overall, however the variation in the median in Figure 7, between the different instrument types is not great. The largest difference being no more than 0.09, which means not more than $10^{0.09} \approx 23\%$ difference between the ratios of the LE5-RD3 instrument combination and those of the LE1-RD3 or the BB-RD3 combinations. The results are therefore not adversely affected by allowing data from the short-period instruments to be included in the data set.

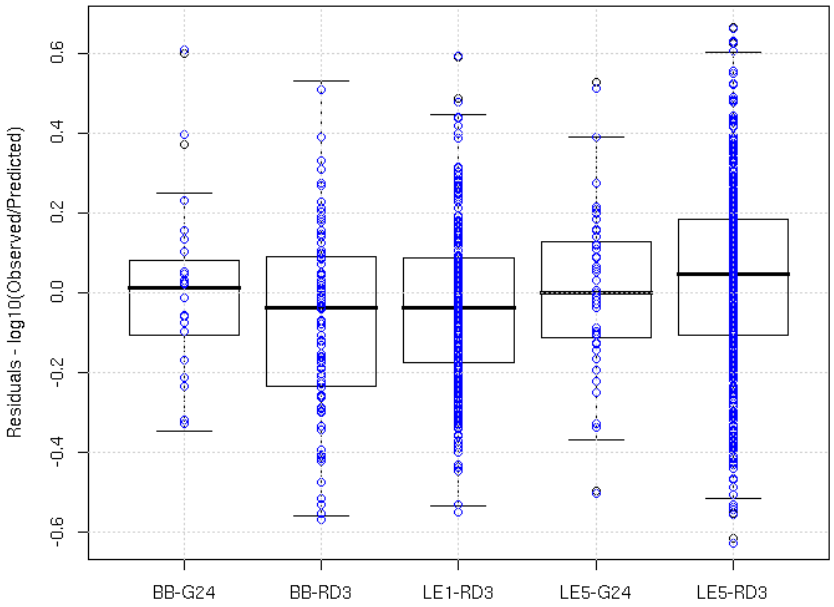

Figure 7. The PGV residuals of 5 different instrument combination classes. BB stands for broad-band. The thick lines show the median of each set and the boxes include measurements from the first to third quartile.

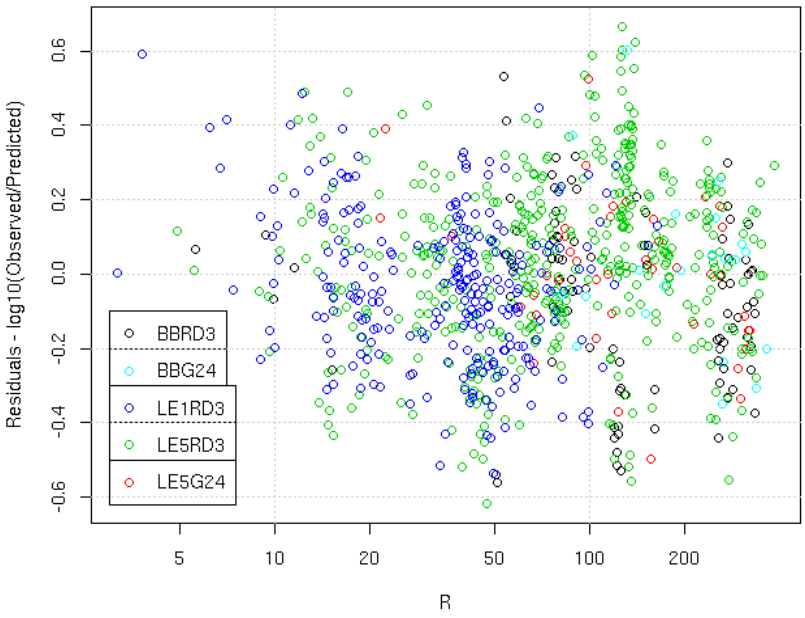

Figure 8. PGV residuals as a function of distance, colored according to the five groups of instrument types.

7 Attenuation relations including a near-source effect

To account for the near-source attenuation described by e.g. Campbell (1981), and to avoid the singularity at the epicenter ($r = 0$) in the attenuation relations for *PGX*, a revision of model A was examined, where $R(r,M)$ is used, rather than just the epicentral distance, r. The model considered is the following:

$$log_{10}(PGX) = a \cdot log_{10}(R(r,M)) + b \cdot M + c \quad (1)$$

with R given by:

$$R = r + k \cdot 10^{gM}, \quad (2)$$

and where r is the distance from epicenter to the point of measurement, k is a parameter to be fitted and g is a value to be chosen or fitted (see below). Before choosing form (2) to represent R, the more simple form

$$R = \sqrt{r^2 + k^2} \quad (3)$$

of Boore *et al* (1997) and Bindi et al. (2006) was tested, so that k was fitted independent of M. However, the least squares fit gave a negligible value for k ($\sim 10^{-7}$ km) and thus, contrary to Joyner and Boore (1981) we find no support for this form while we do find support for form (2) in the data set.

Model (1) with $a = 1$, $d = 0$, $g = b$ and an additional r term, is the model chosen by Fukushima and Tanaka (1990) to model a *PGA* data set. This additional term represents anelastic attenuation, as opposed to the traditional $\log_{10}(r)$ term representing the geometrical spreading in a half space. For our data set the form of Fukushima and Tanaka (1990) gave much higher standard deviations than form (1) with arbitrary a and therefore the latter was chosen. Other authors, such as Ólafsson (1999), Abrahamson and Litehiser (1989) and Boore and Joyner (1997), have also omitted the anelastic term from their models due to spurious values.

When $g = 0.5$ the second term in formula (2) is equal to a multiple of the theoretical fault radius of a circular fault with constant stress drop. The radius is given by

$$C(M_w) = \sqrt[3]{\frac{7M_0}{16\Delta\sigma}} = \sqrt[3]{\frac{7 \cdot 10^{9.1}}{16\Delta\sigma}} 10^{0.5M_w}, \quad (4)$$

where $\Delta\sigma$ is the stress drop (see Appendix A and Hanks Kanamori, 1979). In the last term the seismic moment has been replaced by $10^{1.5M+9.1}$. When $g = 0.5$ the form $R = r + K \cdot C(M)$ gives equivalent results to the form $R = r + k \cdot 10^{g \cdot M}$ when fitted to the data – the only difference between the free parameters k and K is the constant on the right hand side of (4). For a constant stress drop of $\Delta\sigma = 1$ MPa and a fit of model (1) to the *PGV* data with $g = 0.5$ the parameter K is approximately 1.5. Informally speaking, we can say that the transition between near-field and far-field takes place close to 1.5 fault radii away from the epicenter.

We now show why the parameter g should fulfill a constraint in the fitting procedure.

Observe that at $r = 0$ the *PGV* of an event of magnitude M is

$$\log_{10}(PGV) = a\log_{10}(k) + M(b + a \cdot g) + c\,.$$

In order to constrain the *PGV* to be independent of *M* at $r = 0$ we could, in the spirit of Campbell (1981) and Fukushima and Tanaka (1990), choose $g = -b/a$. Let us however look at the predictions at the epicenter more closely.

At $r = 0$ the log-ratio of *PGV* for two events M_2 and M_1 with $M_2 > M_1$ simplifies to:

$$\log_{10}\left(\frac{PGV_2}{PGV_1}\right) = (b + a \cdot g)(M_2 - M_1)\,,$$

so PGV_2 is greater than or equal to PGV_1 when $b+a \cdot g \geq 0$; that is, $g \leq -b/a$ (note that a is negative). In appendix B we show that in this case $PGV_2 \geq PGV_1$ for not only $r = 0$, but for all $r \geq 0$. In order to exclude PGV_2 from being smaller than PGV_1 – a larger event having smaller *PGV* than a smaller event at some distance r – we need to respect the above constraint. Importantly, this constraint also excludes multiple solutions to equation (1) when *PGV* and $r > 0$ are given and M is to be determined.

The global minimum can generally by reached for values of g that may or may not satisfy the constraint, depending on the particular weights chosen in the least squares procedure. Different kinds of weights were tried in the regression process in which case the least squares problem becomes the problem of minimizing

$$\sum_i w_i^2 \left\{\log_{10}(PGX_i) - f(M_i, r_i, ...)\right\}^2,$$

with respect to the parameters of the model f. The weights w_i were generally of the form

$$w_i = \frac{p}{q(M, r)},$$

where p was a normalization constant and usually $q(M,r)$ was a discrete density distribution made to correct for the uneven magnitude or distance distributions in the data set (see Figure 3). Eventually however, all weighting schemes were abandoned since our data set indicates more or less what kind of magnitude distributions one can expect in SW-Iceland. As a counter argument, one might say that our models should pay special attention to the largest earthquakes, but as we shall later see, they fit the M~6.5 recordings very well. By correcting for either the magnitude or distance distributions one runs the risk of putting too much emphasis on erroneous recordings. Moderate weighting schemes do exist however. In their papers, Sharma (1998) and Abrahamson (1989) introduce a weighting method for the correction of uneven distance distributions in their datasets. Equal weights are chosen for a number of distance bins while the size of the bins are chosen somewhat intuitively. The first four distance bins are 2.5 km in size while the remaining bins have equal size on a logarithmic scale.

There are infinitely many ways of choosing weighting schemes. One can apply strict rules or intuition to find the exact method but how do we know which one to choose? Should our choice depend on how close the resulting forecasts of our models are to our expectations or should they depend on numbers like 2.5 (km) that happens to be one fourth of 10? How scientific is

that? Clearly, no one weighting scheme is absolutely correct and therefore we choose to abandon weighting schemes.

When fitting model (1) to the dataset it became clear that the least squares estimate involved a value of g that was very close to the limit case of the constraint $g \leq -b/a$. This limit case, $g = -b/a$, implies magnitude independence at the epicenter as we have argued before. The difference in standard deviation of the least squares fit with g free and standard deviation of g constrained by $g = -b/a$ was only in the fourth significant digit. With the support of this finding, and the long list of authors in Campbell's 1981 paper who believe that peak ground acceleration is independent of magnitude at or very near the rupture surface, we reduce the amount of parameters in model (1) and set $g = -b/a$. Furthermore we introduce a peak ground acceleration model that encompasses this understanding:

$$log_{10}(PGA) = a \cdot log_{10}(R(r,M)) + b \cdot M + c + d \cdot M^2, \quad (5)$$

where R is given by

$$R = r + k \cdot 10^{gM + eM^2} \quad (6)$$

and the parameters g and e are given by: $g = -b/a$ and $e = -d/a$.

The parameters of M and M^2 in model (5) are thus directly linked with the parameters of form (6) to better constrain the behavior in the near-field, and to provide PGA independence of magnitude very close to the epicenter (see Appendix B). As in model B we use a second order term M^2 for the saturation of the PGA relation for large earthquakes.

8 Results

The results for the least squares, non-weighted PGV and PGA models are given by:

$$\log_{10}(PGV) = -1.69 \cdot \log_{10}(r + 0.00299 \cdot 10^{0.621M}) + 1.05 \cdot M - 4.96 \quad (C)$$

$$\log_{10}(PGA) = -2.26 \cdot \log_{10}(r + 0.0309 \cdot 10^{0.569M - 0.0194M^2}) - 0.0437 \cdot M^2 + 1.28 \cdot M - 2.85 \quad (D)$$

where the standard error is 0.223 and 0.302, respectively. The maximum velocity obtainable by model C is 0.21 m/s and the maximum acceleration obtainable by model D is 3.7 m/s^2. Note that the fitting procedure's estimate for g turned out to be of the same order as the exponential parameter in the fault radius formula (4) $-b/a \approx 0.5$.

The residuals of models A to D are approximately normally distributed as has been widely reported in the literature for attenuation models. In Figure 9 an indicative normality plot for model C is shown.

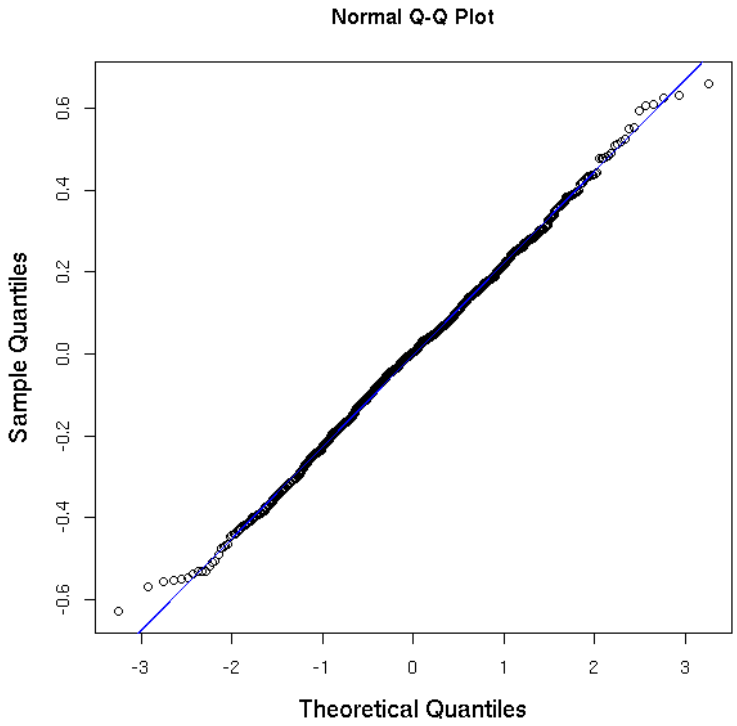

Figure 9. Plot of the log_{10}(PGV) residuals vs. a theoretical normal distribution with the same mean and standard deviation. The residuals of log_{10}(PGX) are approximately normally distributed so the PGX is log-normally distributed.

Two illustrative plots of PGX predictions are shown in Figures 10 and 11 for three different reference events each. The whole data set is plotted in gray in both figures.

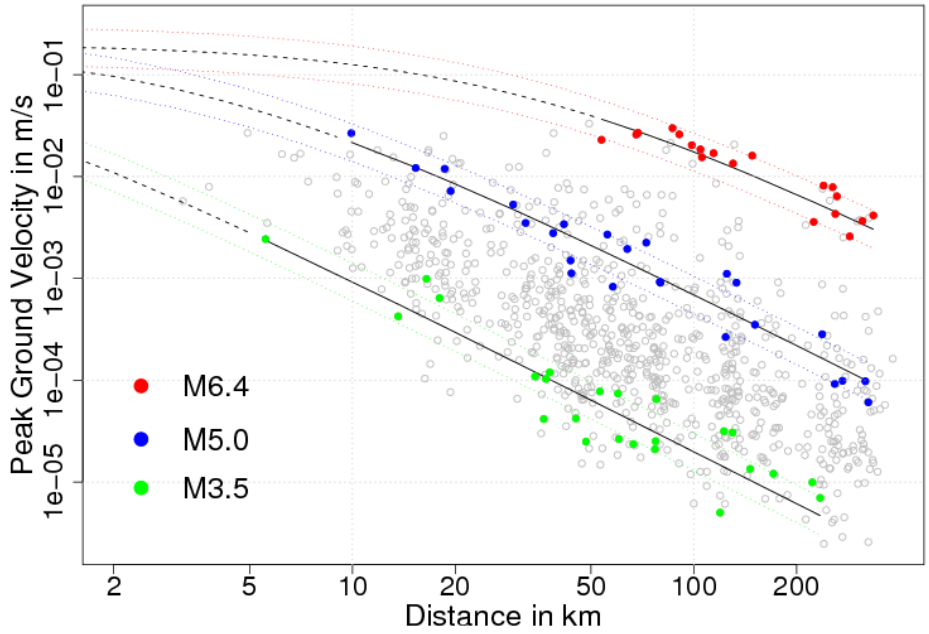

Figure 10. PGV observations for three different events and the corresponding predicted attenuation curves. A solid line is drawn in the distance interval that the observations span. Measurements from other earthquakes are plotted in gray. Standard deviation curves are colored and dotted.

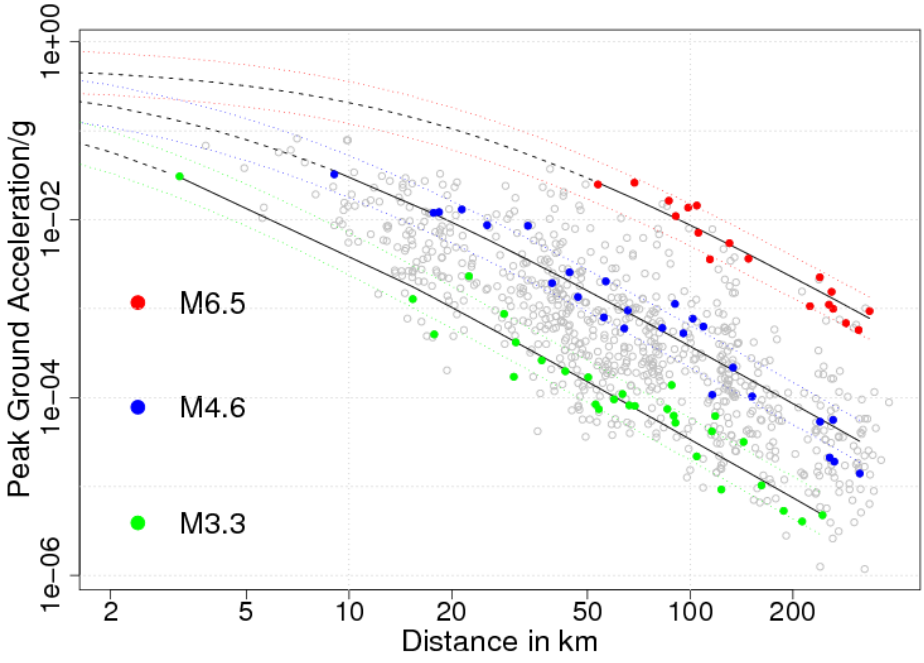

Figure 11. PGA observations for three events, different from those in the previous figure, and the corresponding attenuation curves.

The model predictions for the smaller events in Figures 10 and 11 can be seen to be close to linearity in accordance with the fault radius term in models (1) and (5), which becomes relatively small when M is small and then the non-linearity becomes less prominent.

A comparison between the PGV model of Joyner and Boore (1981) and models A and C can be seen in Figure 12 for the magnitude $M_w(v)$ = 6.5 June 21st, 2000 event. To indicate roughly the standard error of model C, two ± 1 standard deviation lines are drawn in the same figure. The two near-field models agree well in the far-field while they differ by more than a factor of two in the near-field. One rule of thumb states that the maximum *PGV* is 1 m/s for an M7 event, give or take a factor of 2. Our model predicts a maximum of 0.2 m/s for an M7 event so it underestimates the velocity at short distances according to this rule. However, Ólafsson and Sigurbjörnsson (2004) have reported that the Icelandic M~6.5 events had consistently lower *PGA* than similar earthquakes in Europe and North-America. In any case our near-field velocity predictions should be more accurate than those of any log-linear based model, like model A, since they predict infinite velocity at $r = 0$. As can be seen in figure 12, the near-field model describes the data most accurately.

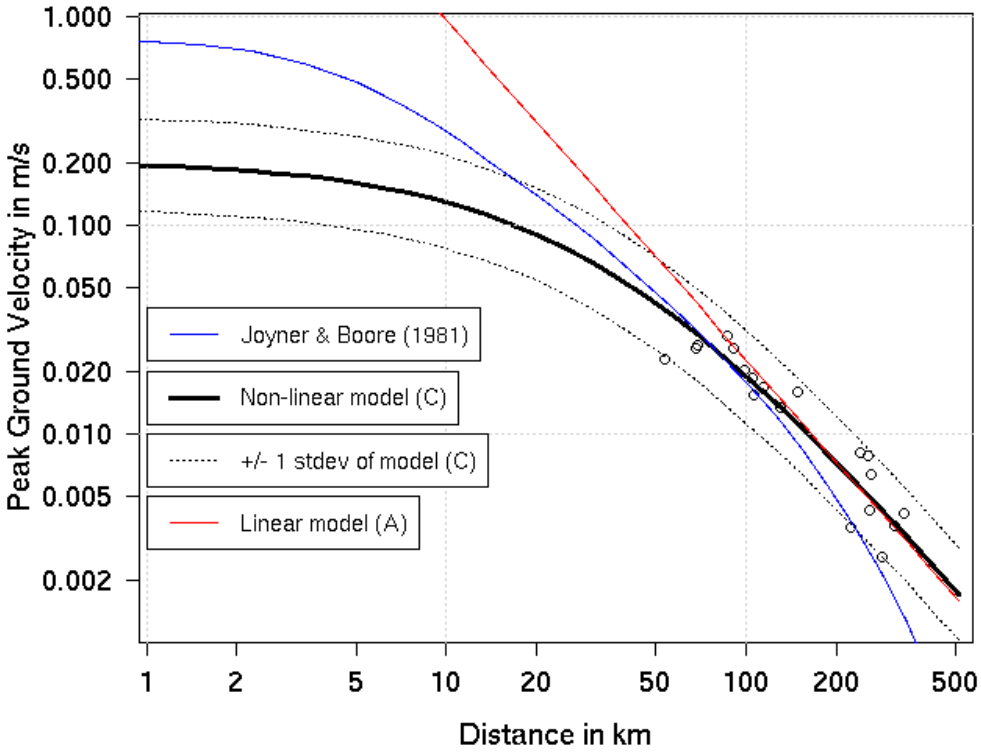

Figure 12. A comparison between three models for an $M_w(v)$6.5 event (black circles). The thick, black line is our model and two +/- 1 standard deviation curves surround it. Our previous log-linear model (A) is plotted in red.

Figure 13 shows a comparison between our *PGA* model D and four horizontal peak ground acceleration models, one vertical-component peak ground acceleration model (Abrahamson and Litehister, 1989), and one theoretical model derived from spectral models (Ólafsson, 1999;

Ólafsson and Sigurbjörnsson, 2004). The inclusion in our data set of the vertical component of acceleration should increase the *PGA* values and model predictions, when in fact they are generally lower than predicted by the other models for the magnitude $M_w(v)$=6.5 reference event, who's measurements are also displayed in the Figure. The Abrahamson and Litehister (1989) model predicts higher far-field acceleration values than the other models, and the Sharma (1998) model (omitted in Figure 13 to reduce clutter) predicts PGA/g above 10^{-2} for all distances. Common to these two studies is the use of a log-distance argument of the form:

$$R = r + exp(gM),$$

rather than form (2) used herein, as well as in the Fukushima and Tanaka (1990) and Campbell (1981) studies. The study by Joyner and Boore (1981) used form (3).

Our model is scaled to M_w, while the comparison models in figure 13 were derived for different types of magnitudes: M_w (Joyner and Boore, Halldórsson and Sveinsson, Ólafsson), M_S (Fukushima and Tanaka, Campbell, Halldórsson, Abrahamson), m_b (Campbell, Abrahamson and Litehister, Halldórsson and Sveinsson) and unknown (Sharma). All the non-Icelandic models were derived using measurements from larger events, typically 5 < M < 8.

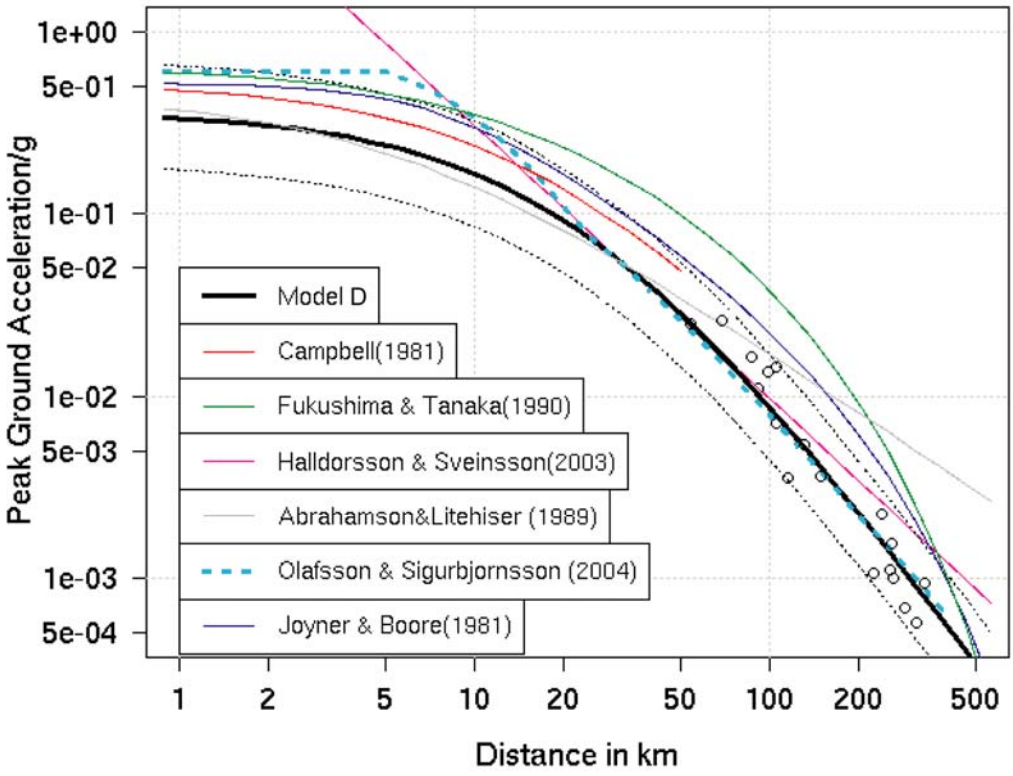

Figure 13. An M6.5 reference event (black circles) and various PGA model predictions. The thick, black line is our model and two +/- 1 standard deviation, dotted curves surround it.

Despite the lack of near-field measurements in our data set the near-field behavior is in very good agreement with the other studies for a 6.5 magnitude earthquake, but generally the non-Icelandic models (Campbell, Fukushima and Tanaka, Abrahamson and Litehister and Joyner

and Boore) predict slightly larger accelerations than the Icelandic models (Halldórsson, Ólafsson and Model C) as well as the observed *PGA* of the reference event. In the report by Ólafsson and Sigurbjörnsson (2004) it is said that the Icelandic M6.5 events were fitted with the theoretical model using the same parameters as with 7 European and N-American events of similar magnitudes, apart from a difference in a spectral decay parameter that effectively lead to a factor √2 difference in the two groups of events. The PGA model is plotted with ± 1 standard deviation curves (0.30– a factor ~2 change) of $\log_{10}$(PGA). The foreign models seem to predict acceleration in the far-field differing by more than 1 standard deviation from the Icelandic models, which are also closer to the observed M6.5 event values.

9 Discussion

The two M6.5 reference events in Figures 12 and 13 are most accurately described by the new PGV and PGA models (C and D) and by the Ólafsson and Sigurbjörnsson relation, even though less than 4% of the observations in our data set correspond to these events. The acceleration model, D shows similar behavior as the models we would like to compare it with – Campbell, Joyner and Boore, and Fukushima and Tanaka–despite the generally lower predictions. Campbell's model is only valid for distances less than 50 km since his data set, of magnitude 5 to 7.7 events, consisted only of observations close to the epicenter (more than 86% were closer than 30 km).

The theoretical relation for attenuation of strong ground motion described by Ólafsson and Sigurbjörnsson (2004), is marked with a dashed blue curve in Figure 13. This model is based on the Brune's source spectra for both the near- and far-field and uses parameters obtained from acceleration records of shallow events; parameters such as shear-wave velocity, corner frequency, rock density, average radiation pattern, source depth, seismic moment, spectral decay factor (near- and far-field), source duration and stress drop. In their study, the near- and far-field relations are separate models, the first of which assumes constant *PGA* within roughly one fault radius. This theoretical model was applied to *PGA* data from the two June 2000 events. The acceleration levels were found to be lower by a factor of 1/√2 for the Icelandic strike-slip records, when compared to European and North-American events of similar sizes and source depths, on normal and oblique faults. This might point to a reason for why the foreign models fail to describe the PGA of our reference events. Ólafsson's and Sigurbjörnsson's model is also the one that fits best, within the one standard deviation region of our model D.

Table 1 shows that the differences between the original local moment magnitudes (M_{Lw}) determined by the SIL system software, and the corresponding CMT magnitudes (M_w) are quite large and therefore our derived magnitude estimates are significantly different from the original ones (see Table 2). The average difference between the original $M_{Lw}(M_0^{SIL})$ and the new estimate $M_w(v)$ is -0.5. Any comparison between our new models and the models of Ágústsson *et al.* (2008) would be flawed to this extent.

The present Eurocode 8 attenuation formula (Halldórsson and Sveinsson, 2003) is:

$$\log_{10}(PGA/g) = -1.50 \cdot \log_{10}(r) + 0.484 \cdot M - 2.16.$$

This relation (H&S) is derived from a set of horizontal PGA measurements using accelerometers, operated by the Earthquake Engineering Research Centre of the University of Iceland. Compared to to our linear model B, the distance coefficient is significangly higher. A likely reason for this discrepancy is the high concentration of intermediate-field observations in the H&S study. Out of the 131 recordings in their data set, only 1 is recorded more than 155 km away from the epicenter and only 4 are further away than 90 km. A total of 99 recordings or 76% of all recordings were measured at distances between 5 and 50 km away from the epicenter (compared to 39% of our data set). To support this claim a simple test was performed. By choosing all observations in our data set from distances less than 150 km and all earthquakes larger than 4.7 in magnitude, a log-linear model with a distance parameter of a = -1.70 was obtained, a 0.38 higher value than in model B! Notice how well the H&S model fits with model D in the distance range 10-100 km in Figure 13.

The H&S model shows similar distance and magnitude parameters to the models by Joyner & Boore (1981) and Bindi *et al.* (2006). All three studies have in common a use of measurements mostly from distances within 100 km from the epicenter and the magnitude parameters in the studies can be seen to vary with the magnitude range used; the lowest value obtained for the largest magnitudes (Joyner and Boore 1981) while the highest value comes from a study with the smallest events (Bindi *et al.* 2006). This trend is reflected in the negative value of the M^2 term in our acceleration models. In models C and D we have seen that the least squares was reached for a value of g that is close to the limit of the constraints, this limit meaning magnitude independence at the epicenter. Fukushima and Tanaka (1990) followed Campbell's (1981) example, by constraining g to this limit case. Since the extent of the near-field increases with the size of the event and as a result, the magnitude independence becomes more dominant, it is no surprise that the magnitude scale saturates for small distances and large events.

Acknowledgements

We would like to thank Einar Kjartansson for his valued discussions and access to his peak ground velocity and acceleration estimates for an earthquake sequence on Reykjanes Peninsula, in January 2008. This work was partly funded by the European Commission under the project SAFER (EVG1-CT-2001-00046). The figures were made by using R and the GMT public domain software (Wessel and Smith, 1998). The figure in Appendix A was made in Matlab.

References

Abrahamson, N.A. and J. J. Litehiser (1989). Attenuation of vertical peak acceleration, *Bull. Seism. Soc. Am.*, **79**: 549–580.

Ágústsson, K., B. Thorbjarnadóttir, K. Vogfjörð (2008). Seismic wave attenuation for earthquakes in SW Iceland – First results. *Icelandic Meteorological Office report* 08005, 13pp.

Bindi D., L. Luzi, F. Pacor, G. Franceschina and R. R. Castro (2006). Ground-Motion Predictions from Empirical Attenuation Relationships versus Recorded Data: The Case of the 1997–1998 Umbria-Marche, Central Italy, Strong-Motion Data Set, *Bull. Seism. Soc. Am.* **96:** 984–1002.

Boore, D., W. Joyner, T. Fumal (1997). Equations for Estimating Horizontal Spectra and Peak Acceleration for North American Earthquakes. Recent Work. *Seismological Research Letters*, **68**: 128–153.

Campbell, K.W (1981). Near-source attenuation for peak horizontal acceleration, *Bull. Seism. Soc. Am.* **71:** 2039–2071.

Dennis, J. E. and Schnabel, R. B (1983). *Numerical Methods for unconstrained Optimization and Nonlinear Equations*. Prentice-Hall, Englewood Cliffs, NJ, 86–103.

Dziewonski, A.M. and J.H. Woodhouse (1983). An experiment in the systematic study of global seismicity: centroid-moment tensor solutions for 201 moderate and large earthquakes of 1981, *J. Geophys. Res.,* 88: 3247-3271. See also http://www.globalcmt.org/

Fukushima, Y. and T. Tanaka (2005). A new attenuation relation for peak horizontal acceleration of strong earthquake ground motion in Japan. *Bull. Seism. Soc. Am.*, **80**: 757–783.

Gerstenberger, M. C., S. Wiemer, L. M. Jones and P. A. Reasenberg (2005). Real-time forecasts of tomorrow's earthquakes in California, *Nature*, **435**(19), 328–331, doi: 10.1038/nature03622.

Goldstein, P. and A. Snoke (2005). SAC availability for the IRIS community, *IRIS DMS Electronic Newsletter*, Vol. VII, no 1, March.

Gudmundsson, G. B., K. S. Vogfjörd and B. S. Thorbjarnardóttir (2006). SIL data status report, in: PREPARED – third periodic report, February 1, 2005 – July 31, 2005. *Icelandic Meteorological Office report,* 06008, Appendix 3, pp 127–131.

Halldórsson, P. and B. I. Sveinsson (2003). Dvínun hröðunar á Íslandi (The attenuation of acceleration in Iceland (in Icelandic). *Icelandic Meteorological Office report,* 03025, 11 pp.

Hanks T. C. and H. Kanamori H (1979). "A moment magnitude scale". *J. Geophys. Res.* **84** (B5): 2348–50.

Hjaltadóttir, S. and K. S. Vogfjörð (2005). Subsurface fault mapping in South-West Iceland by relative location of aftershocks of the June 2000 earthquakes. *Icelandic Meteorological Office Report*, 21, VÍ-ES-01,18pp.

Jakobsdóttir, S. S., G. B. Guðmundsson and R. Stefánsson (2002). Seismicity in Iceland 1991–2000 monitored by the SIL seismic system. *Jökull* **51**, 87–94.

Joyner, W. and D. Boore (1981). Peak horizontal acceleration and velocity from strong-motion records including records from the 1979 Imperial Valley, California, earthquake, *Bull. Seism. Soc. Am.* **71:** 2011–2038.

Joyner, W. and D. Boore (1993). Methods for regression analysis for strong-motion data, *Bull. Seism. Soc. Am.* **83:** 469–487.

Kanamori H. and D. Anderson (1975). Theoretical basis of some empirical relations in Seismology, *Bull. Seism. Soc. Am.* **65:** 1073–1095.

Olafsson, S (1999). Estimation of earthquake-Induced response, *PhD thesis*, Norwegian University of Science and Technology, http://www.afl.hi.is/page/Simon.

Olafsson, S. and R. Sigurbjornsson (2004). Attenuation of Strong Ground Motion in Shallow Earthquakes. *13th World conference on Earthquake Engineering*, Vancouver, Canada. paper No. 1616.

R Development Core Team. R (2007). A language and environment for statistical computing. R Foundation for Statistical Computing, Vienna, Austria. ISBN 3-900051-07-0, URL http://www.R-project.org .

Rögnvaldsson, S. Th. and R. Slunga (1993). Routine fault-plane solutions for local networks: A test with synthetic data, *Bull. Seism. Soc. Am.*, **83**, 1232–1247.

Schnabel, R. B. , Koontz, J. E. and Weiss, B. E (1985). A modular system of algorithms for unconstrained minimization. *ACM Trans. Math. Software*, **11**, 419–440.

Slunga, R., P. Norrman and A. Glans (1984). Seismicity of Southern Sweden – Stockholm: Försvarets Forskningsanstalt, July 1984. *FOA Report*, C2 C20543-T1, 106 p.

Sharma, M.L. (1998). Attenuation relationship for estimation of peak ground horizontal acceleration using data from strong-motion arrays in India, *Bull. Seism. Soc. Am.* **88:** 1063–1069.

Wald, D. J., V. Quitoriano, T. H. Heaton, H. Kanamori, C. W. Scrivner, and C. B. Worden (1999). TriNet ShakeMaps: Rapid Generation of Instrumental Ground Motion and Intensity Maps for Earthquakes in Southern California, *Earthquake Spectra*, **15**, 537–556.

Weisberg, S (1980). *Applied Linear Regression*, Wiley, New York, 283 pp.

Wessel, P. and W.H.F. Smith (1998). New, improved version of Generic Mapping Tools Released. *Eos, Trans. AGU* 79.

Appendix I. The local moment magnitude

The local moment magnitude scale, M_{Lw}, was originally constructed by Slunga *et al.* (1984) to agree with local magnitude scales in Sweden. This magnitude scale, which is used by the SIL system in Iceland, is found from the seismic moment, M_0 in SI units by first calculating m according to:

$$m = \log_{10}(M_0) - 10,$$

and then, given m, using the appropriate case below (Gudmundsson *et al.*, 2006):

$M_{Lw} = m$ if $m \leq a$

$M_{Lw} = 2.0 + (m-a)\cdot 0.9$ $a < m \leq a+b$

$M_{Lw} = 3.0 + (m-a-b)\cdot 0.8$ $a+b < m \leq a+b+c$

$M_{Lw} = 4.6 + (m-a-b-c)\cdot 0.7$ $a+b+c < m \leq a+b+c+d$

$M_{Lw} = 5.4 + (m-a-b-c-d)\cdot 0.5$ $a+b+c+d < m \leq a+b+c+d+e$

$M_{Lw} = 5.9 + (m-a-b-c-d-e)\cdot 0.4$ $a+b+c+d+e < m \leq a+b+c+d+e+f$

$M_{Lw} = 6.3 + (m-a-b-c-d-e-f)\cdot 0.35$ $a+b+c+d+e+f < m$

Here, $a = 2$, $b = 1/0.9$, $c = 1.6/0.8$, $d = 0.8/0.7$ and $e = f = 1$.

In SI-units the moment magnitude scale proposed by Hanks and Kanamori (1979) is defined by:

$$M_w = \frac{2}{3}\left(\log_{10}(M_0) - 9.1\right)$$

In the figure below the two magnitudes are compared. As the figure demonstrates, the magnitude scales are the same at M = 1.8 and M = 6.5. For the magnitude range: $1.8 < M < 6.5$, M_{Lw} is greater than M_w, while outside this range M_w is larger.

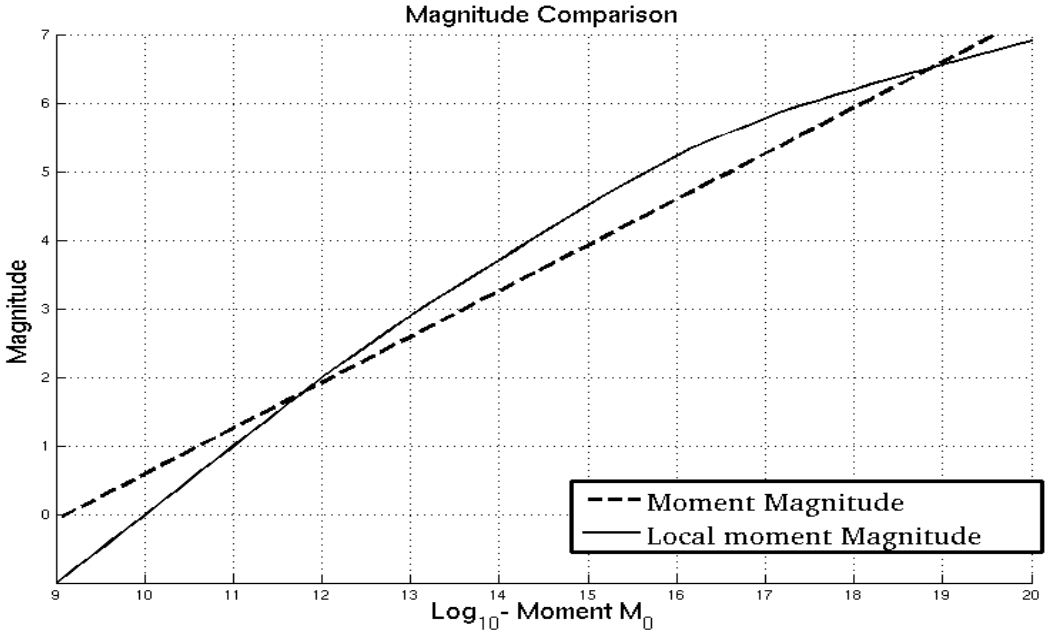

Appendix II. Near-field constraint

In the model section we showed that magnitude independence of PGV at the epicenter brings about a constraint on g, g = -b/*a*. Similarly, for PGA at r = 0 we have

$$\log_{10}(PGA) = a\log_{10}(k) + a\cdot g\cdot M + a\cdot e\cdot M^2 + b\cdot M + d\cdot M^2$$
$$= a\log_{10}(k) + M(b + a\cdot g) + M^2(d + a\cdot e)$$

and thus we would require b+*a*·g = 0 and d+*a*·e = 0 in the acceleration case.

We now investigate whether an M_2 event can have smaller ground motion at the same distance as an M_1 event if $M_2 > M_1$ and find constraints to prevent this from occurring. We already saw in the model section that in the case of velocity, $\log_{10}(PGV_2/PGV_1) \geq 0$ when b+*a*·g ≥ 0 and r = 0. Treating both models (1) and (5) at the same time (for PGV just put d = e = 0) we have, more generally, at r = 0 that

$$\log_{10}\left(\frac{PGX_2}{PGX_1}\right) = a\log_{10}\left(\frac{k\cdot 10^{gM_2+eM_2^2}}{k\cdot 10^{gM_1+eM_1^2}}\right) + b(M_2 - M_1) + d(M_2^2 - M_1^2) =$$

$$(b + a\cdot g)(M_2 - M_1) + (d + a\cdot e)(M_2^2 - M_1^2) = (M_2 - M_1)\left(b + a\cdot g + (d + a\cdot e)(M_2 + M_1)\right) \geq 0$$

where the inequality sign holds if b+*a*·g ≥ 0 and d+*a*·e ≥ 0. In the case of acceleration it is possible that these conditions do not suffice for PGA_2 to be larger than PGA_1, but that is the (here) irrelevant case of $M_2+M_1 < 0$.

What if r > 0? is PGX_2 always larger than PGX_1 when the above constraints on g and e hold?

Yes, when r > 0 the log-ratio takes the form

$$\log_{10}\left(\frac{PGX_2}{PGX_1}\right) = -a\log_{10}\left(\frac{r + k\cdot 10^{gM_1+eM_1^2}}{r + k\cdot 10^{gM_2+eM_2^2}}\right) + b(M_2 - M_1) + d(M_2^2 - M_1^2),$$

where the denominator and numerator of the logarithm on the right side have been switched in order to obtain the positive parameter -*a*. By differentiating with respect to r we can obtain information on how the PGX ratio depends on r. Since -*a* is positive, -*a*·$\log_{10}(\cdot)$ is an increasing function and therefore it suffices to differentiate its argument:

$$\frac{d}{dr}\left(\frac{r + k\cdot 10^{gM_1+eM_1^2}}{r + k\cdot 10^{gM_2+eM_2^2}}\right) = k\frac{10^{gM_2+eM_2^2} - 10^{gM_1+eM_1^2}}{(r + k\cdot 10^{gM_1+eM_1^2})^2}.$$

In the case of PGV, e = 0 and then, since $M_2 > M_1$, g > 0 and k > 0 [1)], the derivative is always positive and therefore the PGV ratio strictly increases with r. This means that the minimum of the ratio PGV_2 / PGV_1 is reached when r = 0, where it is greater than or equal to 1 if the conditions on g is satisfied.

---

1) When k = 0 the nonlinear part vanishes and we obtain models A and B again. We have already mentioned that the data does not support a model in which g = 0, furthermore g < 0 or k < 0 are not physically plausible, nor does the least-squares method return negative values for these parameters. The assumptions of g > 0 and k > 0 are therefore realistic to say the least.

The same condition on g holds for the model of Fukushima and Tanaka (1990) in which an additional 'anelastic' r-term enters the equation, since in the above derivations it cancels out like the parameter c does.

In the case of PGA the above derivative is always positive if $gM_2+eM_2^2 \geq gM_1+eM_1^2$. This is certainly correct in the case of independence of M at r = 0, since the above inequality becomes $bM_2+dM_2^2 \geq bM_1+dM_1^2$ which states that the magnitude dependence of model (5) is a positive one – when M increases, PGA increases.

More generally, when the independence assumption is not taken for granted, this inequality can be informally understood to mean that fault radius increases with magnitude – the second term in form (6) should increase with magnitude.

The conditions on g and e ensure that a magnitude M_2 event has larger PGX than a smaller event with magnitude M_1 for all r > 0. When this condition is satisfied, PGX_2 and PGX_1 can be equal only in the special case of $b+a\cdot g+(d+a\cdot e)(M_2+M_1) = 0$ and then only at r = 0.

By equating PGX_2/PGX_1 to one in the above r dependent formula and then solving for r, it is possible to find at what distance two events could theoretically have the same PGX. In general, two PGX(r,·) curves whose magnitudes are M and M+δ, with $\delta>0$, will intersect at a distance

$$r = k \cdot 10^{gM+eM^2} \frac{10^{\frac{\delta}{a}(b+ag+(d+ae)(2M+\delta))}-1}{1-10^{\frac{\delta}{a}(b+d(2M+\delta))}}.$$

This formula simplifies when we consider the velocity case with d = e = 0. When the distance is negative it means that the curves do not intersect (PGX of one event is never equal to the other). This can only happen when $b+a\cdot g+(d+a\cdot e)(M_2+M_1) > 0$ since then the above numerator is negative while the denominator is positive (keep in mind that *a* is negative).

Appendix III. PGV and PGA versus distance for all events

In the following figures all events have been grouped according to locations and their recordings plotted with a fit of models C (PGV) and D (PGA). Six events are located in the SISZ, eight on Reykjanes Peninsula, five in the southern part of the Hengill region, and the remaining 26 in the northern part of the Hengill region (see Figure 1 and text for details).

The legends in the figures below have the format 'M_{Lw}(v) YYYYMMDD $M_w(M_0)$'. All events can be identified by these three parameters.

For each event, solid lines are drawn in the distance range spanned by the recordings, while dashed lines show extrapolations from the minimum distance recording.

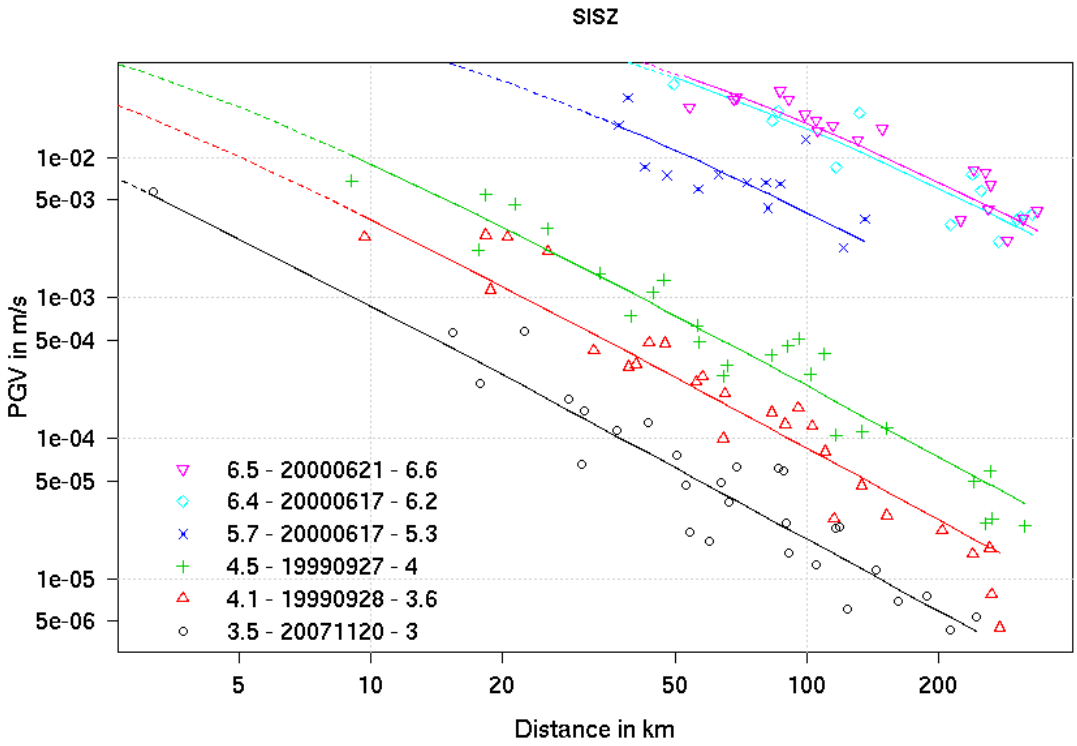
SISZ
PGV in m/s
1e-02
5e-03
1e-03
5e-04
1e-04
5e-05
1e-05
5e-06
6.5 - 20000621 - 6.6
6.4 - 20000617 - 6.2
5.7 - 20000617 - 5.3
4.5 - 19990927 - 4
4.1 - 19990928 - 3.6
3.5 - 20071120 - 3
5
10
20
50
100
200
Distance in km

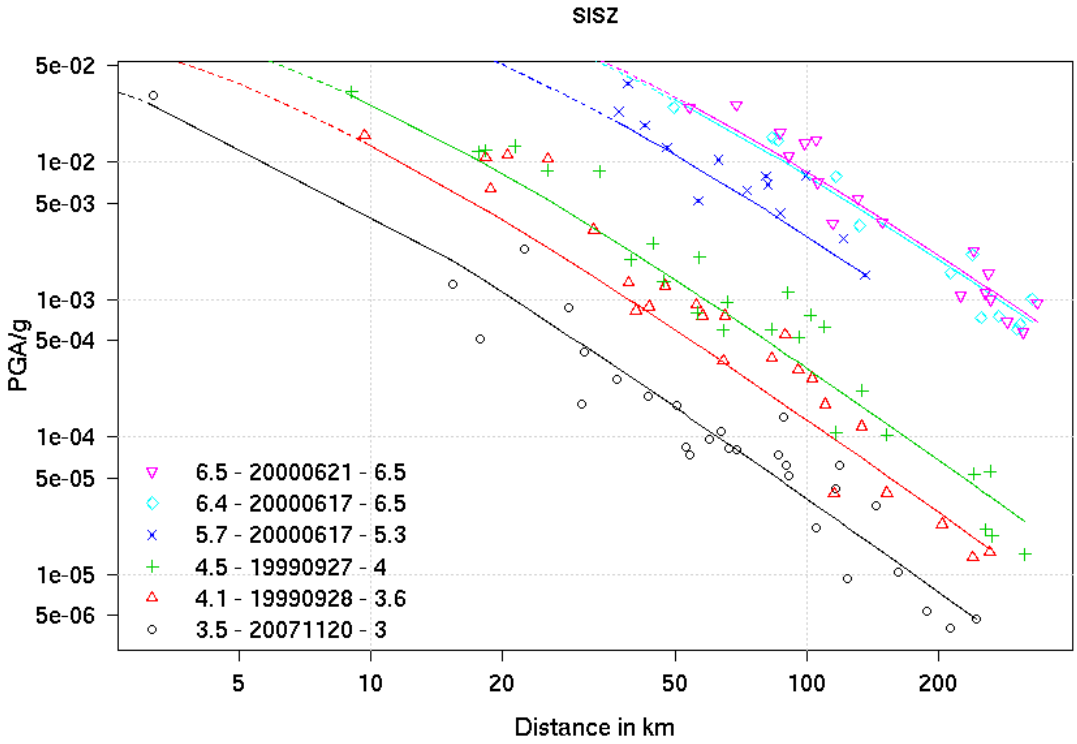
SISZ
PGA/g
5e-02
1e-02
5e-03
1e-03
5e-04
1e-04
5e-05
1e-05
5e-06
6.5 - 20000621 - 6.5
6.4 - 20000617 - 6.5
5.7 - 20000617 - 5.3
4.5 - 19990927 - 4
4.1 - 19990928 - 3.6
3.5 - 20071120 - 3
5
10
20
50
100
200
Distance in km

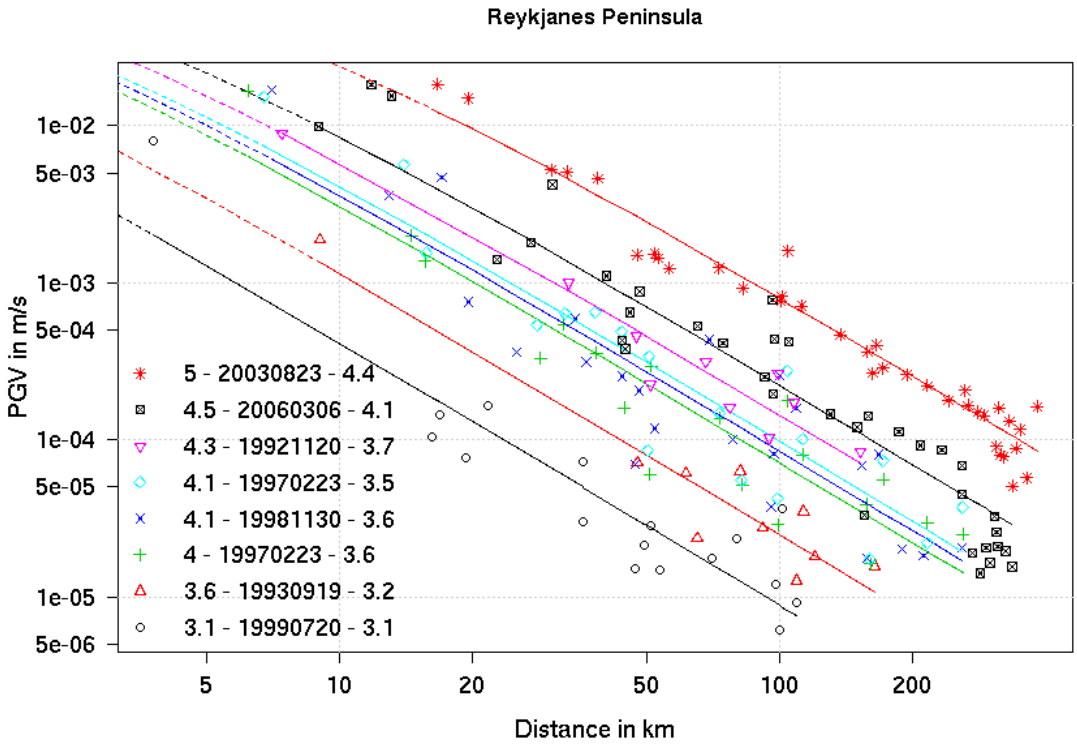
Reykjanes Peninsula
PGV in m/s
1e-02
5e-03
1e-03
5e-04
1e-04
5e-05
1e-05
5e-06
5 - 20030823 - 4.4
4.5 - 20060306 - 4.1
4.3 - 19921120 - 3.7
4.1 - 19970223 - 3.5
4.1 - 19981130 - 3.6
4 - 19970223 - 3.6
3.6 - 19930919 - 3.2
3.1 - 19990720 - 3.1
5
10
20
50
100
200
Distance in km

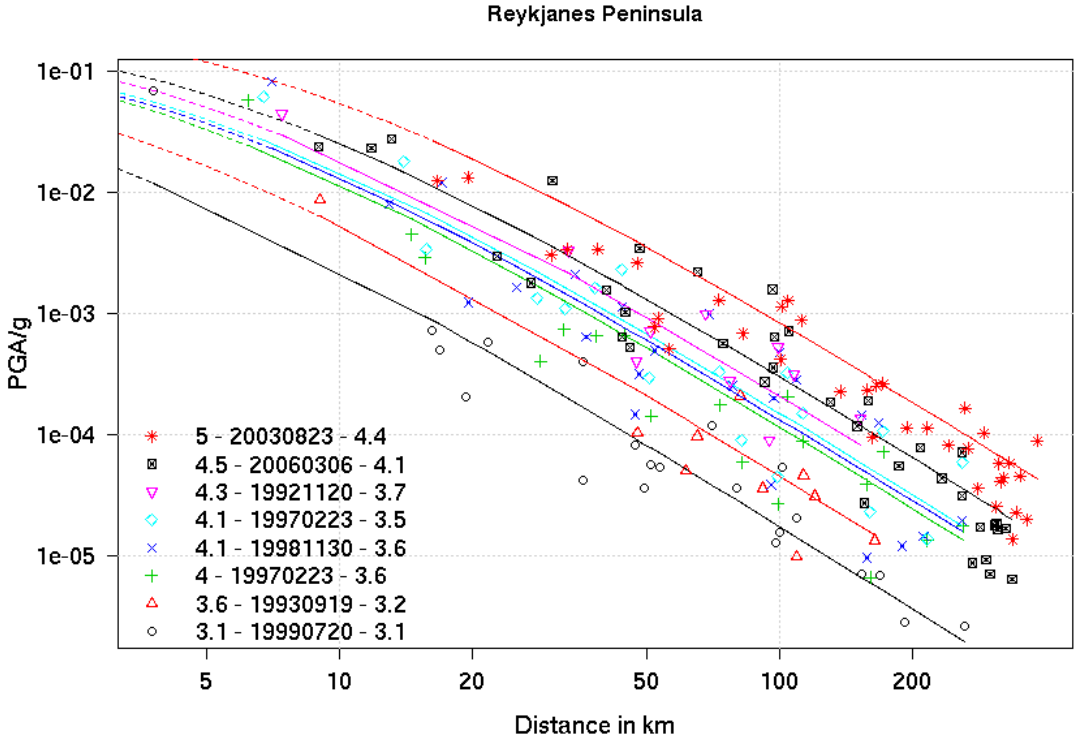
Reykjanes Peninsula
PGA/g
1e-01
1e-02
1e-03
1e-04
1e-05
5 - 20030823 - 4.4
4.5 - 20060306 - 4.1
4.3 - 19921120 - 3.7
4.1 - 19970223 - 3.5
4.1 - 19981130 - 3.6
4 - 19970223 - 3.6
3.6 - 19930919 - 3.2
3.1 - 19990720 - 3.1
5
10
20
50
100
200
Distance in km

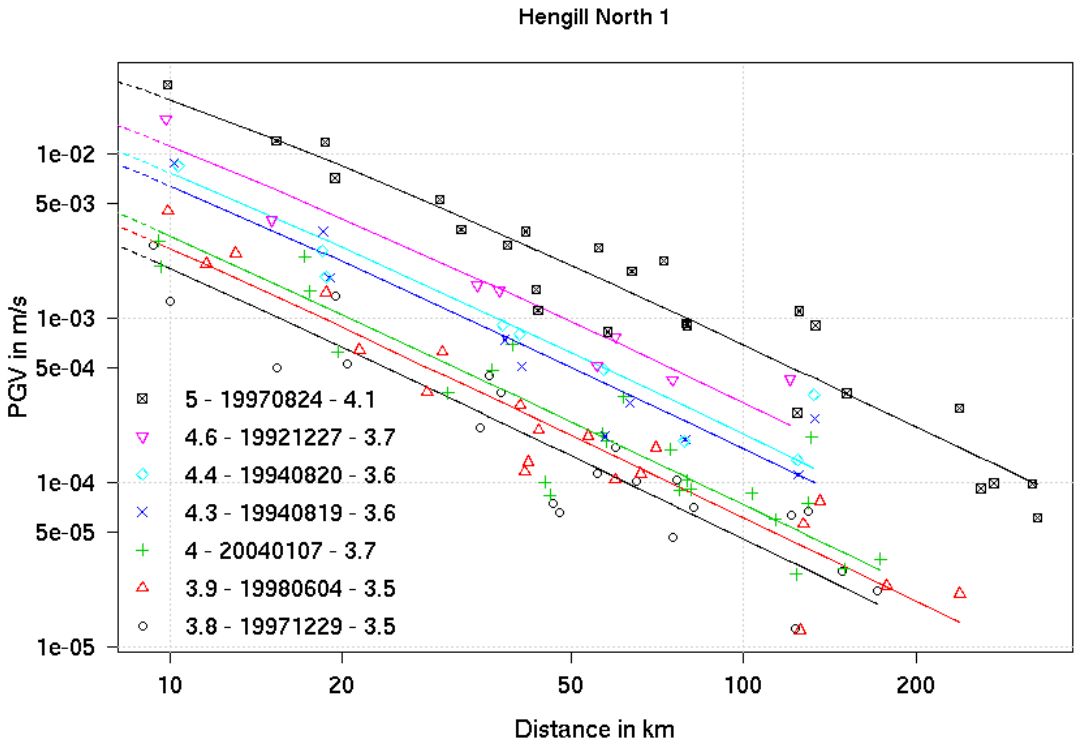
Hengill North 1
PGV in m/s
1e-02
5e-03
1e-03
5e-04
1e-04
5e-05
1e-05
5 - 19970824 - 4.1
4.6 - 19921227 - 3.7
4.4 - 19940820 - 3.6
4.3 - 19940819 - 3.6
4 - 20040107 - 3.7
3.9 - 19980604 - 3.5
3.8 - 19971229 - 3.5
10
20
50
100
200
Distance in km

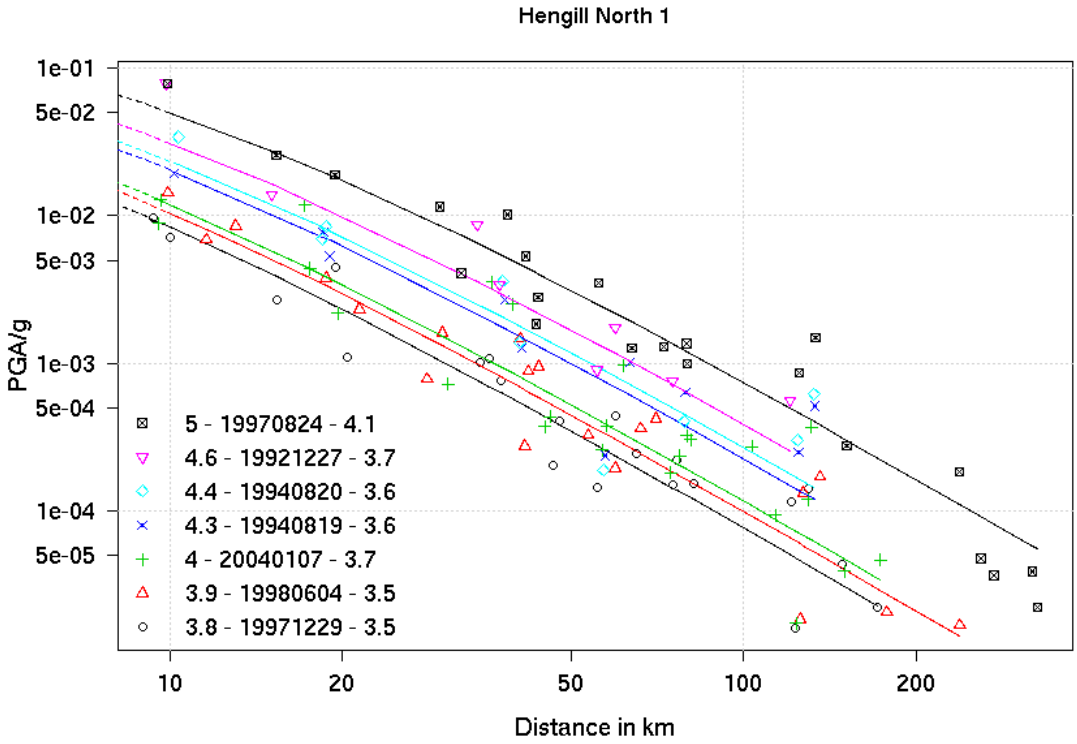
Hengill North 1
PGA/g
1e-01
5e-02
1e-02
5e-03
1e-03
5e-04
1e-04
5e-05
5 - 19970824 - 4.1
4.6 - 19921227 - 3.7
4.4 - 19940820 - 3.6
4.3 - 19940819 - 3.6
4 - 20040107 - 3.7
3.9 - 19980604 - 3.5
3.8 - 19971229 - 3.5
10
20
50
100
200
Distance in km

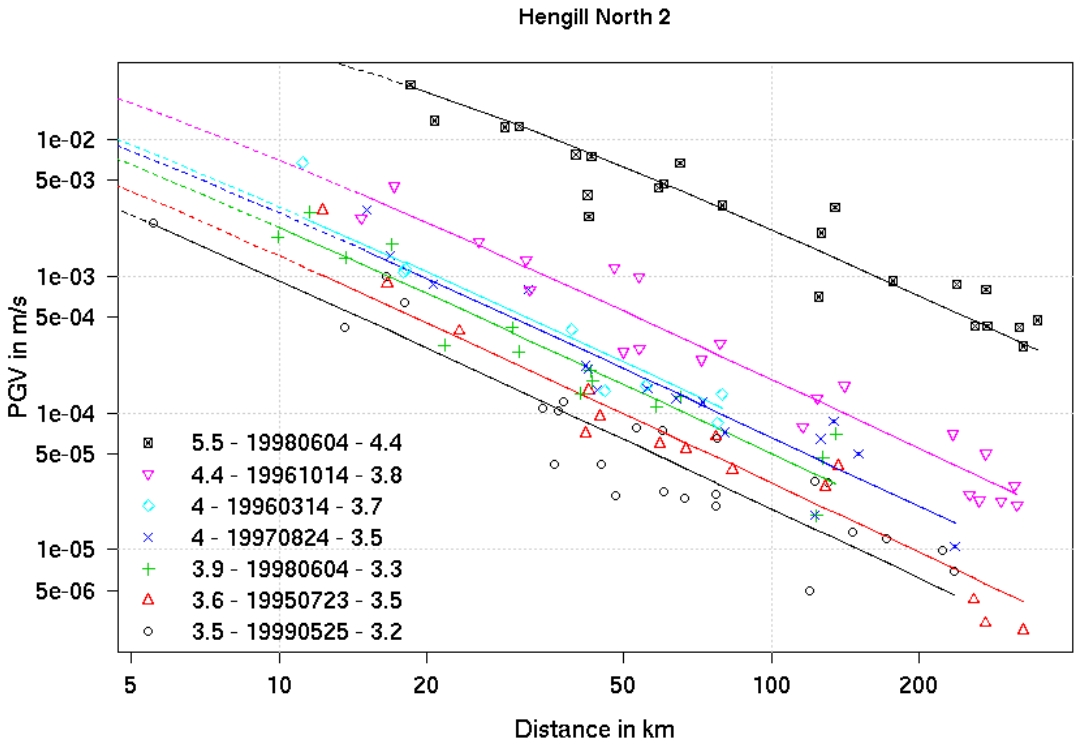
Hengill North 2
PGV in m/s
1e-02
5e-03
1e-03
5e-04
1e-04
5e-05
1e-05
5e-06
5.5 - 19980604 - 4.4
4.4 - 19961014 - 3.8
4 - 19960314 - 3.7
4 - 19970824 - 3.5
3.9 - 19980604 - 3.3
3.6 - 19950723 - 3.5
3.5 - 19990525 - 3.2
5
10
20
50
100
200
Distance in km

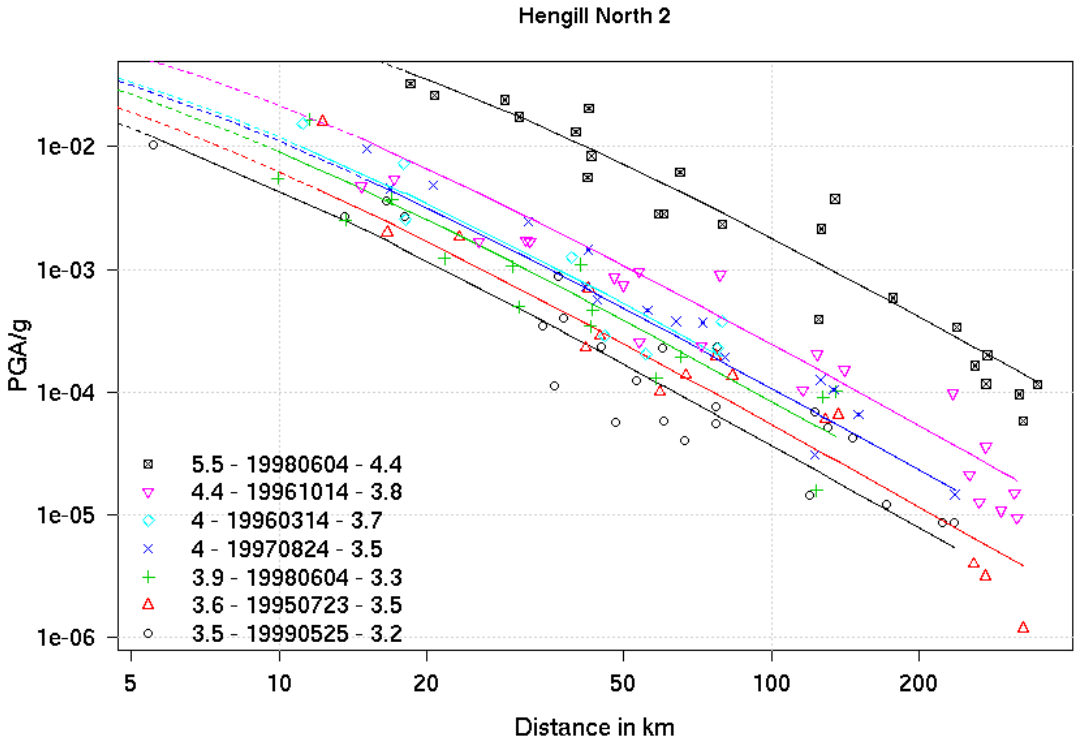
Hengill North 2
PGA/g
1e-02
1e-03
1e-04
1e-05
1e-06
5.5 - 19980604 - 4.4
4.4 - 19961014 - 3.8
4 - 19960314 - 3.7
4 - 19970824 - 3.5
3.9 - 19980604 - 3.3
3.6 - 19950723 - 3.5
3.5 - 19990525 - 3.2
5
10
20
50
100
200
Distance in km

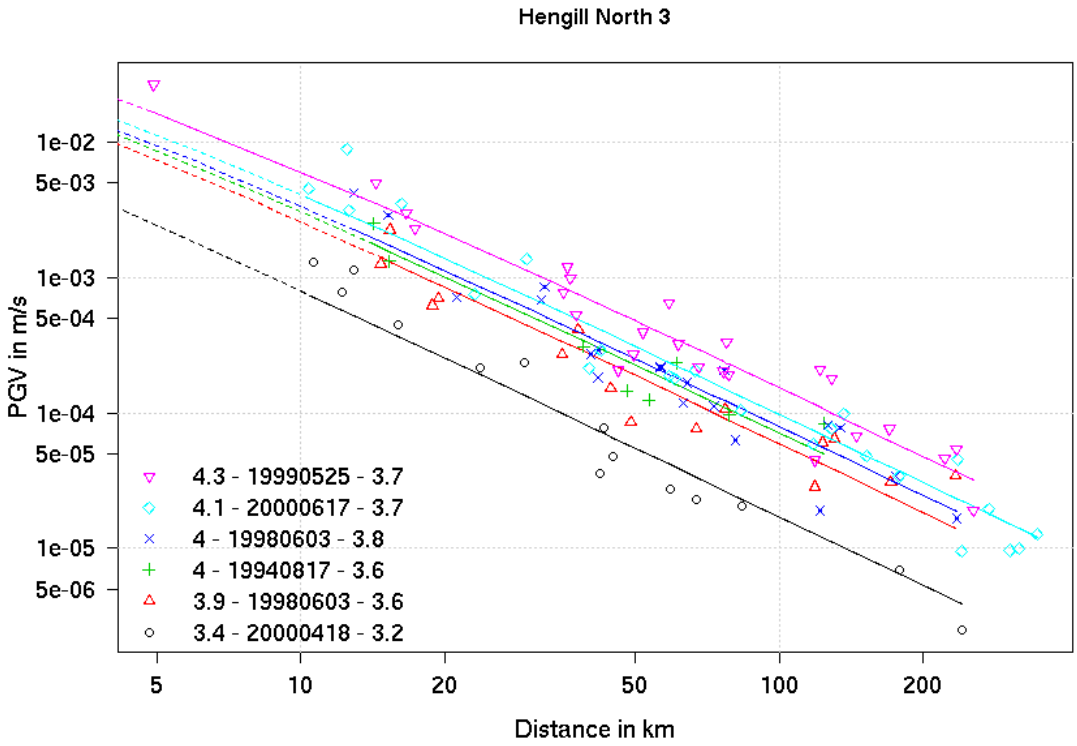
Hengill North 3
PGV in m/s
1e-02
5e-03
1e-03
5e-04
1e-04
5e-05
1e-05
5e-06
4.3 - 19990525 - 3.7
4.1 - 20000617 - 3.7
4 - 19980603 - 3.8
4 - 19940817 - 3.6
3.9 - 19980603 - 3.6
3.4 - 20000418 - 3.2
5
10
20
50
100
200
Distance in km

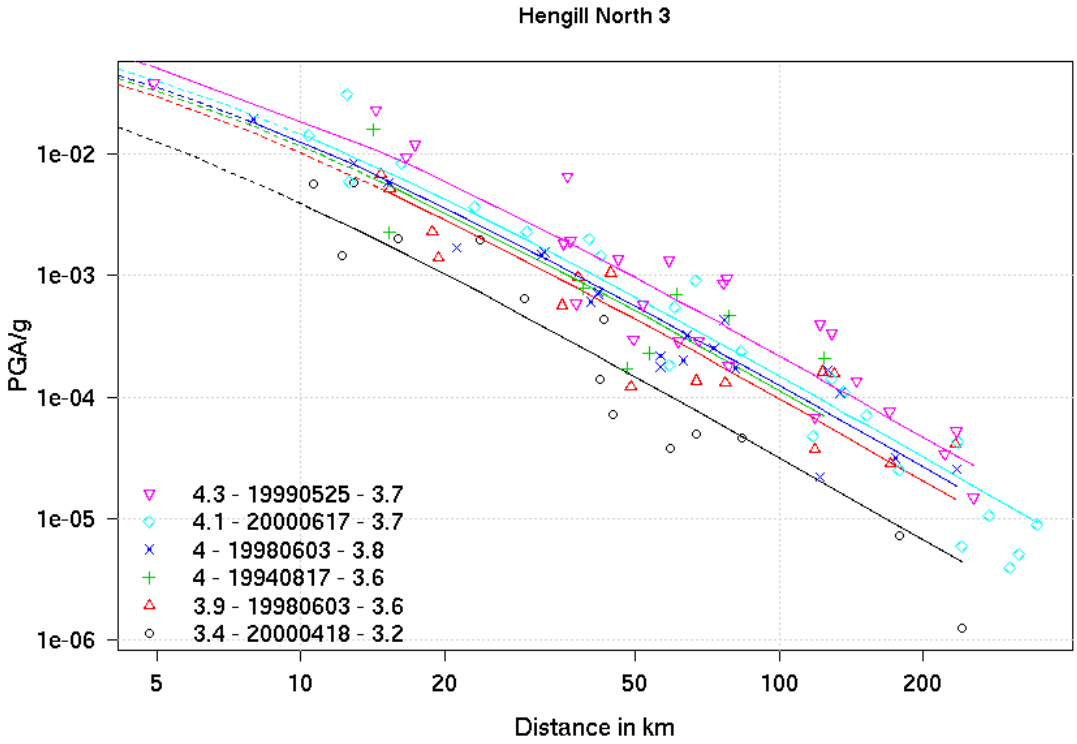
Hengill North 3
PGA/g
1e-02
1e-03
1e-04
1e-05
1e-06
4.3 - 19990525 - 3.7
4.1 - 20000617 - 3.7
4 - 19980603 - 3.8
4 - 19940817 - 3.6
3.9 - 19980603 - 3.6
3.4 - 20000418 - 3.2
5
10
20
50
100
200
Distance in km

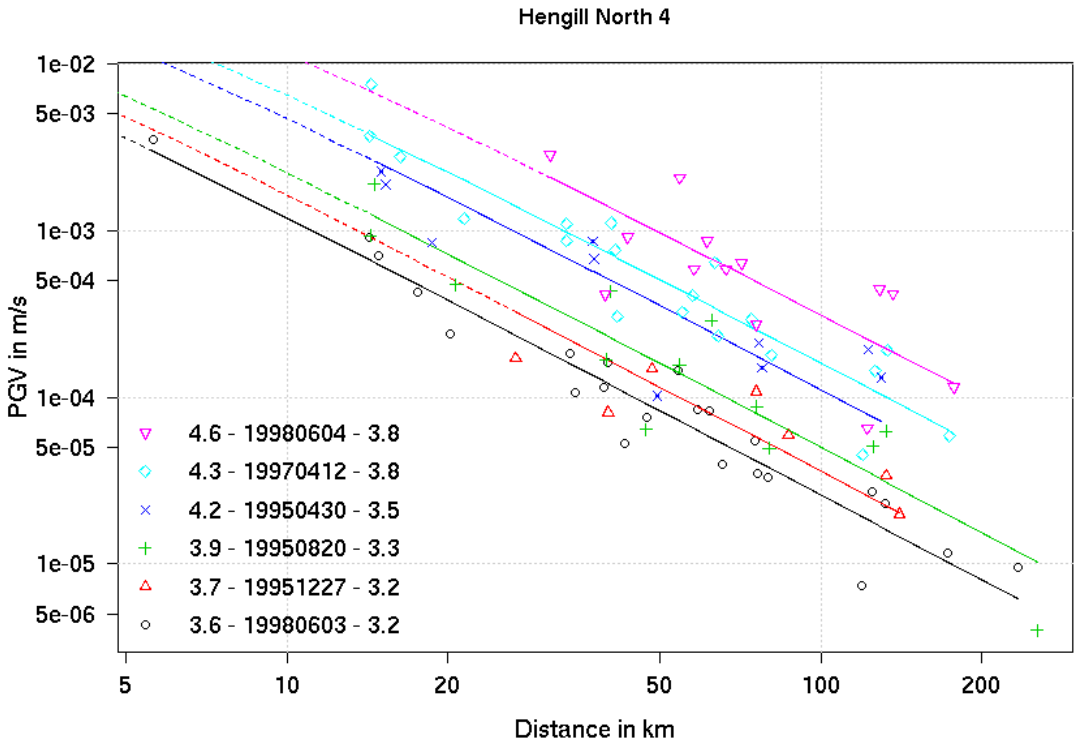
Hengill North 4
PGV in m/s
1e-02
5e-03
1e-03
5e-04
1e-04
5e-05
1e-05
5e-06
4.6 - 19980604 - 3.8
4.3 - 19970412 - 3.8
4.2 - 19950430 - 3.5
3.9 - 19950820 - 3.3
3.7 - 19951227 - 3.2
3.6 - 19980603 - 3.2
5
10
20
50
100
200
Distance in km

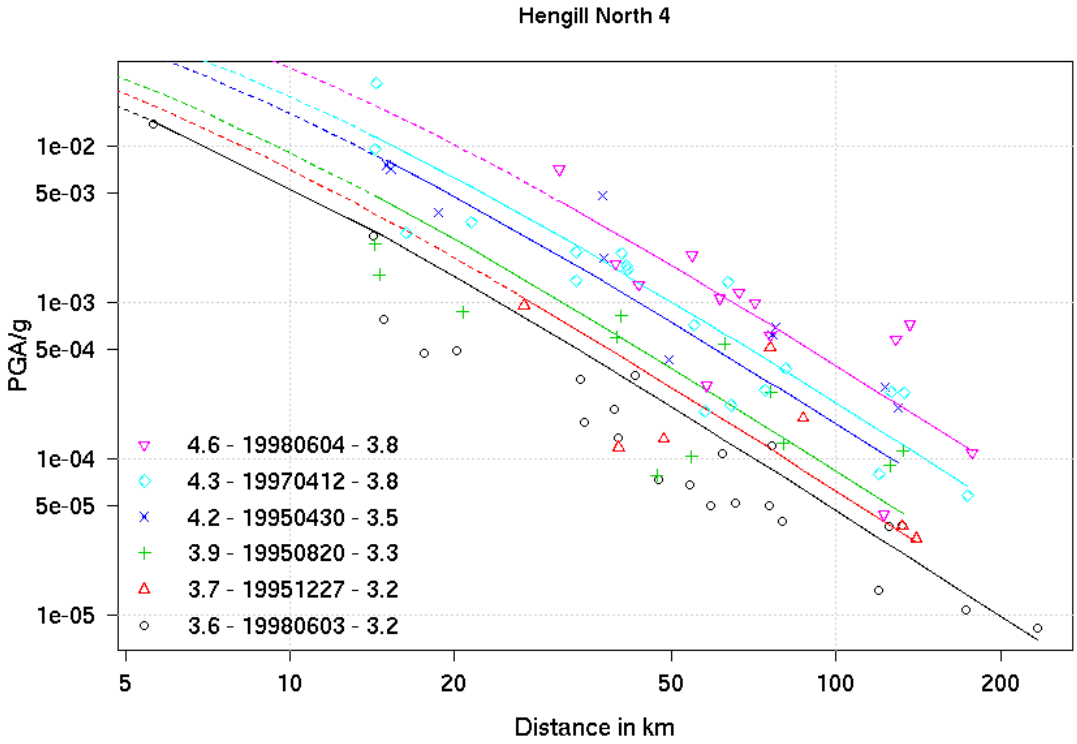
Hengill North 4
PGA/g
1e-02
5e-03
1e-03
5e-04
1e-04
5e-05
1e-05
4.6 - 19980604 - 3.8
4.3 - 19970412 - 3.8
4.2 - 19950430 - 3.5
3.9 - 19950820 - 3.3
3.7 - 19951227 - 3.2
3.6 - 19980603 - 3.2
5
10
20
50
100
200
Distance in km

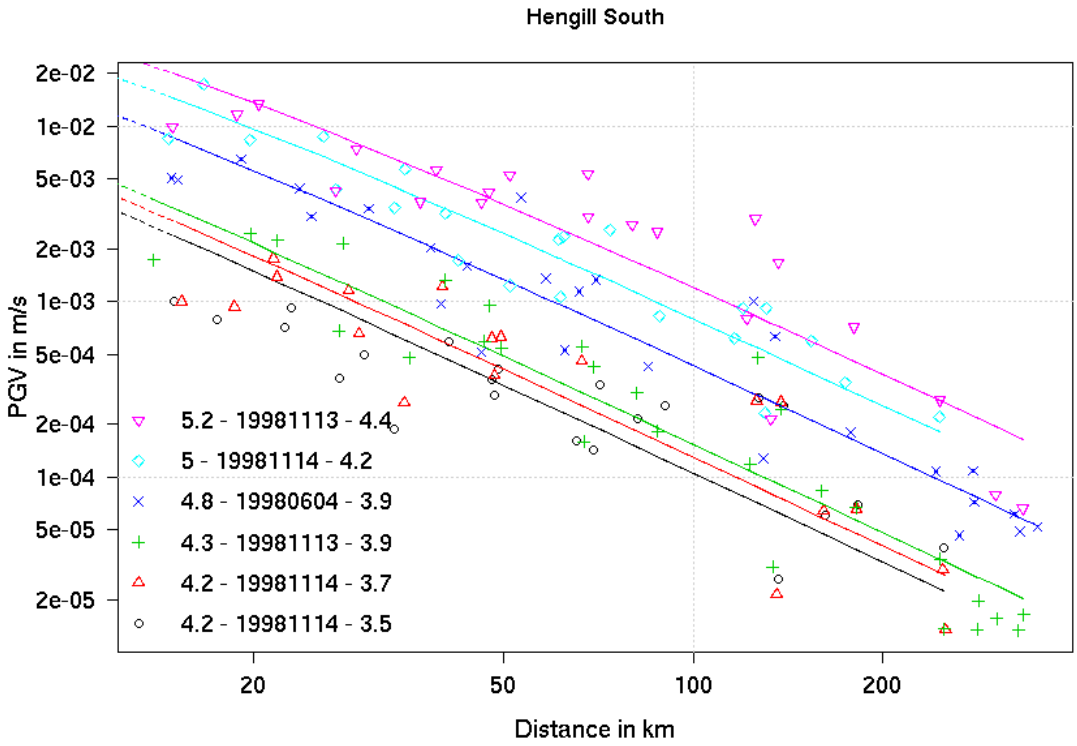
Hengill South
PGV in m/s
2e-02
1e-02
5e-03
2e-03
1e-03
5e-04
2e-04
1e-04
5e-05
2e-05
5.2 - 19981113 - 4.4
5 - 19981114 - 4.2
4.8 - 19980604 - 3.9
4.3 - 19981113 - 3.9
4.2 - 19981114 - 3.7
4.2 - 19981114 - 3.5
20
50
100
200
Distance in km

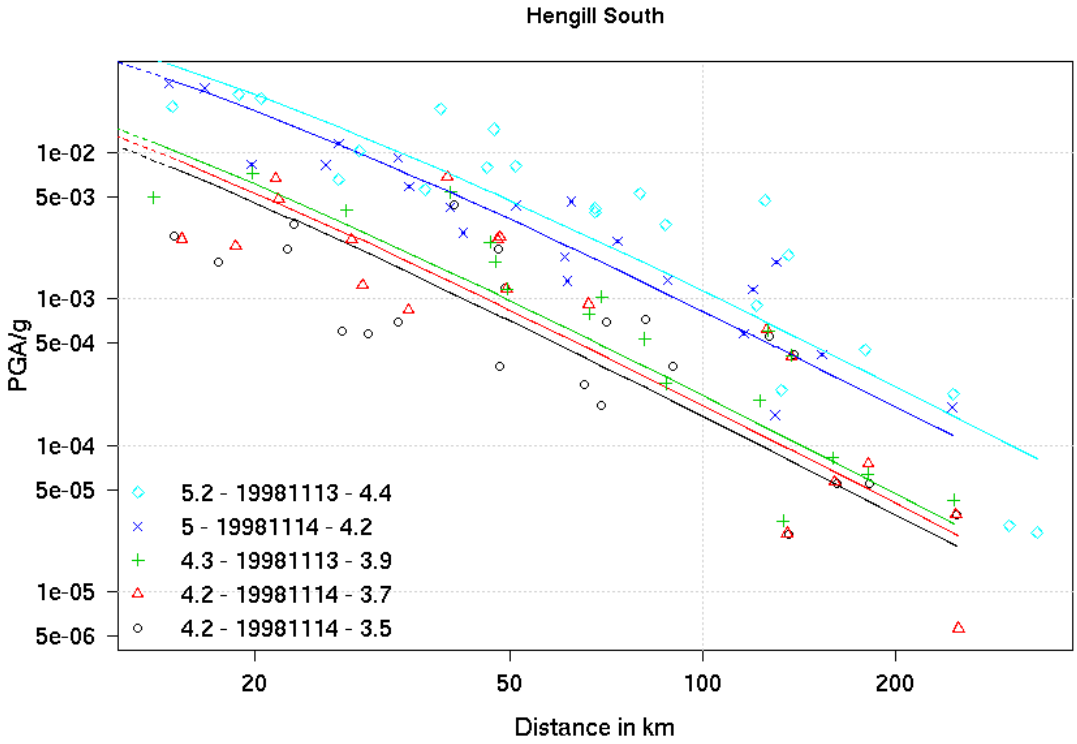
Hengill South
PGA/g
1e-02
5e-03
1e-03
5e-04
1e-04
5e-05
1e-05
5e-06
5.2 - 19981113 - 4.4
5 - 19981114 - 4.2
4.3 - 19981113 - 3.9
4.2 - 19981114 - 3.7
4.2 - 19981114 - 3.5
20
50
100
200
Distance in km